www.sciencemag.org/content/343/6175/1133/suppl/DC1

Supplementary Materials for

# Structural Basis for Heavy Metal Detoxification by an Atm1-Type ABC Exporter

Jonas Y. Lee, Janet G. Yang, Daniel Zhitnitsky, Oded Lewinson, Douglas C. Rees*

*Corresponding author. E-mail: dcrees@caltech.edu

Published 7 March 2014, *Science* **343**, 1133 (2014)
DOI: 10.1126/science.1246489

**This PDF file includes:**

## Materials and Methods

Summary: Finding the Best Target and Maximizing the Resolution of Data Collection

The crystal structure of *Novosphingobium aromaticivorans* Atm1 (*Na*Atm1) was solved following an initial screen of 40 different Atm1 genes. Of these 40, we were able to successfully clone 34, express 18, and crystallize 4 of these gene products in 7 different crystal forms. Of the 7 different crystal forms, 4 did not diffract, 2 diffracted to 7-10 Å resolution, and 1 (NaAtm1) diffracted anisotropically to 3.5-4 Å resolution in one direction. The best diffracting crystals were improved by growing larger crystals and optimizing the cryocooling conditions to yield a resolution of either 2.9 Å ($(I/\sigma I) > 2$) or 3.2 Å (R-merge > 66%) (Table S1). To further improve the usable resolution and quality of the resulting electron density maps, we utilized Karplus' CC* (Pearson's correlation coefficient) based data cutoff approach *(40)* (Table S2), with Liu's method of maximizing the anomalous $CC_{1/2}$ signal through high redundancy data collection *(41)*, and found that the mean $I/\sigma I$), $CC_{1/2}$, and usable resolution were optimized with a data multiplicity of greater than 15. For the initial model building and refinement, the initial resolution limit was set as $CC_{1/2}$ ~ 20% based on the data merging statistics from Aimless (Table S3). For the final refinement and publication, the final resolution limit was reduced by CC* analysis against unmerged intensities in Phenix package (Table S2) satisfying Karplus' CC* against CC-work and CC-free criteria, as well as, R-free of the highest resolution shell against the refined structure being less than or equal to ~50%.

Cloning, Purification, and Crystallization

Forty genes from various organisms including *Novosphingobium aromaticivorans* DSM 12444 were selected by searching for proteins containing the conserved domain ATM1 (NCBI CDD:34862) in the NCBI GenPept database (*42*). The full length gene (Accession ABD27067) was PCR amplified from purified genomic DNAs and cloned into a pJL-H6 ligation independent cloning vector (*43*) which adds a 6-His tag on the carboxy terminus.

The target was expressed in *Escherichia coli* BL21(DE3) cells grown in ZYM-5052 autoinduction media (*44*). The expressed cell paste was resuspended in lysis buffer containing 20 mM Tris pH 7.5, 0.1 M NaCl, 0.1 mg/mL hen egg lysozyme, 0.01 mg/mL DNaseI, and 1 mM PMSF. The resuspended cells were lysed using a M-110L pneumatic microfluidizer (Microfluidics). Unlysed cells were removed by centrifugation at 10,000 x g, and membranes containing *Na*Atm1p were separated by ultracentrifugation at 100,000 x g. The membrane pellets were resuspended in lysis buffer and stored at -80$^{o}$C until use.

The protein was extracted from the resuspended membrane pellet by directly adding 0.25% w/v (final concentration) each of n-dodecyl-N,N-dimethylamine-N-oxide (LDAO), 3-[(3-cholamidopropyl)dimethylammonio]-2-hydroxy-1-propanesulfonate (CHAPSO), n-octyl-β-D-glucopyranoside (OG), and undecanoyl-N-hydroxyethylglucamide (HEGA-11). Although these four detergents were individually poor in extracting protein from membranes and in maintaining homogeneity, their mixture was unexpectedly found to be quite effective in both aspects. Unextracted membranes were removed by ultracentrifugation at 100,000 x g. *Na*Atm1p was purified by immobilized nickel ion-affinity chromatography using a HisTrap HP 5 mL column (GE Healthcare) followed by size-exclusion chromatography using a HiLoad 16/60 Superdex-200 prep grade column (GE Healthcare) equilibrated with buffer containing 20 mM Tris pH 7.5, 0.1 M NaCl, 0.025% w/v LDAO, 0.025% w/v CHAPSO, 0.025% w/v OG, and 0.025% w/v HEGA-11. The eluted sample was pooled and concentrated to a final concentration of 10 mg/mL using a 100 kDa molecular-weight cutoff spin concentrator. 20 mM (final conc.) of sodium citrate at pH 7.5 was added to the final protein solution as a crystallization aid.

The initial crystallization trials were performed using the sparse-matrix method (*45*) using Index (Hampton Research), and MemGold (Molecular Dimensions) screens. All drops were set up in 96-well MRC sitting-drop crystallization plates (Hampton Research) with 0.7 uL of protein mixed with 0.7 uL of precipitant equilibrated with 50 uL of precipitant and incubated at 4 $^{o}$C. Six initial hits were found. The best diffracting

crystals were found from 100 mM sodium citrate pH 5.4, 200 mM magnesium acetate, and 12% w/v polyethylene glycol 5,000 monomethyl ether after optimizing MemGold condition A12. Crystals appeared within a week and grew to a typical size of 100 μm x 50 μm, with some crystals as large as 250 μm x 150 μm (~20% of crystallizing drops) observed within two to three weeks. Selenomethionine substituted *Na*Atm1 crystals were prepared the same way as the native crystals except that the expression utilized B834(DEC) cells grown in PASM-5052 autoinduction media (*44*).

X-Ray Data Collection and Structure Determination

Crystals were harvested from the crystallization plate using a nylon loop and soaked in cryoprotectant solution containing 100 mM sodium citrate pH 5.4, 200 mM magnesium acetate, and polyethylene glycol 5,000 monomethyl ether in three steps of 10, 18, and 25% before flash-freezing in liquid nitrogen. The crystals were soaked with substrates by adding 1 to 5 mM of substrate into the cryoprotectant solution. The diffraction data was collected at the Stanford Synchrotron Radiation Laboratory beamline 12-2 equipped with a PILATUS 6M PAD detector. The data was collected to maximize the signal (mean(I/σI)) in the highest resolution outer shell while maintaining an overall data completeness of greater than 95% by collecting 900˚ or 1080˚ data sets with 0.15˚ or 0.2˚ oscillation steps at the maximum allowable attenuation (97%) before predicted radiation damage occurred (Table S1).

The diffraction data were indexed and integrated using XDS (*46*), and scaled using Aimless with the CCP4i interface (*47*) with default options. The experimental phases were determined by AutoSol in the Phenix package (*48*) with default options except Kramers-Kronig constants were calculated by the SSRL BluIce software from the Se-edge MAD scan, and input manually. For the apo model, all residues in the transmembrane domains (residue number $\leq$ 350) were built manually using Coot by placing helices and assigning the sequence manually (*49*). The nucleotide binding domain structure was generated using Sav1866 (PDB ID 2HYD) NBD structure as a template using Sculptor in Phenix, and manually placed using Coot.

The sequence registry was initially checked using the heavy atoms sites in the Pt derivative, and subsequently from the positions of the SeMet sites, which independently established the positions of methionine residues. Additional validation was obtained from the locations of mercury sites observed in anomalous difference Fourier maps for $HgCl_2$ soaked crystals of *Na*Atm1 variants with Cys incorporated at either residues 143, 200 and 293, in addition to a composite omit map calculated with AutoBuild in Phenix (*48*) at 2.35 Å resolution.

The apo structure was refined using Phenix.Refine in Phenix (*48*) with the following refinement strategies: "XYZ coordinates," "real-space," "TLS parameters," "occupancies," and "individual B-factors." The following restraints were used: "NCS restraints," "secondary structure restraints," and "experimental phase restraints" along with "update waters" function in the later refinement stages. The TLS groups were determined by Find_tls_groups in Phenix. All restraints were used with the default option, which included torsion-angle NCS restraints with a 15 degree limit and a 2.5 degree sigma. We verified that the use of two-fold NCS restraint between subunits in the homodimer did not significantly bias R-free by removing the NCS restraints for the GSSG bound structure. Removing the NCS restraints marginally lowered R-work (by 0.11%) and raised R-free (by 0.13%) relative to the NCS restrained refinement. Nevertheless, implementing the NCS restraints gave a better geometry in terms of Ramachandran (1.4% more in the favored region) and rotamer (0.53% fewer outliers) distributions, which minimized the need to manually place geometry restraints on disordered loop regions for all the refined structures.

Phases for the substrate bound structures were calculated after rigid-body refinement of the protein chains in the apo structure using Refmac5 (*47*). All cif libraries for the ligands were generated using eLBOW in Phenix (*48*). The ligands were manually placed using Coot. All ligand bound structures were refined using Phenix.Refine in Phenix (*48*) with the same option as the apo structure described above except experimental phase restraints were removed. CC*, CC-work, and CC-free were calculated using Phenix

using the unmerged intensity outputs generated from Aimless in CCP4 to determine the final resolution cutoff. The final refinements for all the structures were done using Phenix.Refine with the same option as the above without the real-space refinement strategy and experimental phase restraints.

Structural Superpositions

The Secondary Structure Matching (SSM) program (*50*) implemented in CCP4i (*47*) was used to superimpose TM1-2, TM4-5, and TM3&6 of structurally characterized ABC exporters onto the corresponding elements of the *Na*Atm1 structure (Fig. 4A). The rmsd in Cα positions for the nine independent chains relative to the *Na*Atm1 structure were found to be: TM1-2 (ave 2.06 Å, min/max = 1.60 - 2.61 Å, with an average of 99/118 residues used in the superimposition), TM4-5 (ave 1.89 Å, min/max = 1.41 - 2.48 Å, with an average of 106/114 residues used in the superimposition), and TM3&6 (ave 2.65 Å, min/max = 2.20 - 3.11 Å, with an average of 82/94 residues used in the superimposition).

Measuring Michaelis-Menten Constants of Various Substrates

Reduced glutathione (GSH), oxidized glutathione (GSSG), S-methyl glutathione, S-hexyl glutathione, S-lactoyl glutathione, glutathione S-sulfonic acid, γ-Glu-Cys peptide, Cys-Gly peptide, sodium acetate, sodium propionate, and all amino acids used in the study were purchased from Sigma-Aldrich. Ophthalmic acid was purchased from VWR. Bimane conjugated GSH was synthesized by mixing monobromobimane (Sigma-Aldrich) with reduced GSH in a 1 to 1 molar ratio respectively and incubating overnight at room temperature. The completion of the reaction and the depletion of free monobromobimane were confirmed by adding additional reduced GSH and measuring the change in fluorescence at 478 nm using a Tecan Infinite 200 microplate reader. Dinitrobenzene conjugated GSH was synthesized by reacting 2,4-dinitrochlorobenzene (Sigma-Aldrich) with reduced GSH in a 1 to 1 molar ratio respectively with glutathione S-transferase from equine liver (Sigma-Aldrich). The completion of the reaction and the depletion of free 2,4-dinitrochlorobenzene were confirmed by adding additional reduced GSH and

measuring the change in absorbance at 340 nm. The glutathione-mercury complex was synthesized by mixing reduced GSH and mercury(II) chloride (Sigma-Aldrich) in 2 to 1 molar ratio respectively and incubating at room temperature overnight. The glutathione-silver complex was synthesized by mixing reduced GSH and silver(I) nitrate (Sigma-Aldrich) in 2 to 1 molar ratio respectively, adjusting the pH to 7.0, incubating at room temperature overnight, then boiling at 100$^{o}$C for 5 minutes. All substrates were adjusted to pH 7-8 with NaOH or HCl before use.

The ATPase activity of *Na*Atm1 was determined from the rate of appearance of free phosphate generated by the hydrolysis of ATP using the Invitrogen EnzCheck Phosphate Assay kit implemented in a 96-well plate format with a Tecan Infinite 200 microplate reader. Protein concentrations of 100 to 250 nM, quantitated using the Bradford reagent, were used for each assay. All reactions were performed on a 100 uL scale in 20 mM Tris pH 7.5, 100 mM NaCl, 5 mM EDTA, 0.32% w/v CHAPSO, 1 mM ATP, and 0.015% w/v n-dodecyl-β-D-maltopyranoside (DDM). The reaction was started by adding 10 mM (final conc.) of $MgCl_2$. S-hexyl GSH measurements were done in duplicates, and all other measurements were done in triplicate. The kinetic parameters were determined by a nonlinear least squares fit using the program using the program R (*51*), fitting the ATPase data to a Michaelis-Menten model with a constant basal ATPase activity:

$$\frac{v}{E_T} = \frac{k_{cat}[S]}{K_m + [S]} + k_{basal}$$

where $k_{basal}$ is measured to be 8.8 $\pm$ 0.8 min$^{-1}$ in 1 mM ATP.

Proteoliposome GSSG Transport Assay

Membrane vesicles were prepared from the fractioned *E. coli* cell membranes used for protein purification. Membranes were washed with 20 mM Tris pH 7.5, 500 mM NaCl, pelleted, and resuspended at 20 mg/ml in transport buffer (20 mM Tris pH 7.5, 100 mM NaCl). Membrane suspensions were then sonicated on ice using a Misonix S-4000 ultrasonic processor, power 60, for three cycles at 15s on/45 s off. Vesicles were subjected to 5 cycles of freeze-thaw to scramble the orientation of *Na*Atm1 in the membrane (*52*). Vesicles were extruded 11 times through a 400-nm polycarbonate filter

and centrifuged at 70k rpm for 25 min in a TLA 100.3 rotor. Pellets were washed 3x and resuspended to 20 mg/ml in transport buffer. Transport reactions contained 17 mM Tris, pH 7.5, 85 mM NaCl, 15 mg/ml membranes, 0.5 mM GSSG, and 10 mM MgATP. Reactions were incubated at 30 ˚C and initiated by the addition of ATP. 150 ul samples were removed at various time points and added to 1 ml ice-cold 0.85x transport buffer. Samples were immediately pelleted and washed three times, and solubilized to 22.5 mg/mL membranes in 0.9x transport buffer with 1% w/v DDM. The amount of GSSG was quantified using the glutathione assay kit from Sigma-Aldrich based on the 5,5'-dithiobis-(2-nitrobenzoic acid)-based glutathione reductase recycling assay (*53*). The concentration of *Na*Atm1 was estimated from the intensity of the relevant band on a Coomassie stained SDS-PAGE gel.

Metal Sensitivity Assay

Metal sensitive *E. coli* strains GG44 ($Cu^{+}$/$Ag^{+}$ sensitive) and GG48 ($Zn^{+2}$/$Cd^{2+}$/$Hg^{2+}$ sensitive) were used (*30, 54*). Cells transformed with the indicated plasmids were grown at 37˚C in LB medium containing ampicillin (100 µg/ml) and kanamycin (30 µg/ml). The cells were then diluted to an $OD_{600}$ of 0.05 in 150 µl of the same media, containing L-arabinose (0.02 %) and in the presence or absence of metal salts ($CuSO_4$, $ZnSO_4$ or $CdCl_2$). No protection was conferred by *Na*Atm1 against $Cu^{+2}$, $Zn^{+2}$ or $Cd^{+2}$ toxicity (data not shown). Metal sensitivities with $AgNO_3$ and $HgCl_2$ were performed in a similar manner, but in Davis minimal medium. Growth was monitored continuously for 12 hours in a Tecan Infinite 200 microplate reader.

**References**


1. R. Lill, G. Kispal, Mitochondrial ABC transporters. *Res. Microbiol.* **152**, 331–340 (2001). doi:10.1016/S0923-2508(01)01204-9 Medline

2. I. B. Holland, S. P. C. Cole, K. Kuchler, C. F. Higgins, *ABC Proteins: From Bacteria to Man* (Academic Press, London, 2003).

3. A. Zutz, S. Gompf, H. Schägger, R. Tampé, Mitochondrial ABC proteins in health and disease. *Biochim. Biophys. Acta* **1787**, 681–690 (2009). doi:10.1016/j.bbabio.2009.02.009 Medline

4. H. Ye, T. A. Rouault, Human iron-sulfur cluster assembly, cellular iron homeostasis, and disease. *Biochemistry* **49**, 4945–4956 (2010). doi:10.1021/bi1004798 Medline

5. R. Lill, B. Hoffmann, S. Molik, A. J. Pierik, N. Rietzschel, O. Stehling, M. A. Uzarska, H. Webert, C. Wilbrecht, U. Mühlenhoff, The role of mitochondria in cellular iron-sulfur protein biogenesis and iron metabolism. *Biochim. Biophys. Acta* **1823**, 1491–1508 (2012). doi:10.1016/j.bbamcr.2012.05.009 Medline

6. G. Kispal, P. Csere, B. Guiard, R. Lill, The ABC transporter Atm1p is required for mitochondrial iron homeostasis. *FEBS Lett.* **418**, 346–350 (1997). doi:10.1016/S0014-5793(97)01414-2 Medline

7. S. Bekri, G. Kispal, H. Lange, E. Fitzsimons, J. Tolmie, R. Lill, D. F. Bishop, Human ABC7 transporter: Gene structure and mutation causing X-linked sideroblastic anemia with ataxia with disruption of cytosolic iron-sulfur protein maturation. *Blood* **96**, 3256–3264 (2000). Medline

8. P. C. Krishnamurthy, G. Du, Y. Fukuda, D. Sun, J. Sampath, K. E. Mercer, J. Wang, B. Sosa-Pineda, K. G. Murti, J. D. Schuetz, Identification of a mammalian mitochondrial porphyrin transporter. *Nature* **443**, 586–589 (2006). Medline

9. H. Chavan, M. Oruganti, P. Krishnamurthy, The ATP-binding cassette transporter ABCB6 is induced by arsenic and protects against arsenic cytotoxicity. *Toxicol. Sci.* **120**, 519–528 (2011). doi:10.1093/toxsci/kfr008 Medline

10. M. Tsuchida, Y. Emi, Y. Kida, M. Sakaguchi, Human ABC transporter isoform B6 (ABCB6) localizes primarily in the Golgi apparatus. *Biochem. Biophys. Res. Commun.* **369**, 369–375 (2008). doi:10.1016/j.bbrc.2008.02.027 Medline

11. K. Kiss, A. Brozik, N. Kucsma, A. Toth, M. Gera, L. Berry, A. Vallentin, H. Vial, M. Vidal, G. Szakacs, Shifting the paradigm: The putative mitochondrial protein ABCB6 resides in the lysosomes of cells and in the plasma membrane of erythrocytes. *PLOS ONE* **7**, e37378 (2012). doi:10.1371/journal.pone.0037378 Medline

12. J. K. Paterson, S. Shukla, C. M. Black, T. Tachiwada, S. Garfield, S. Wincovitch, D. N. Ernst, A. Agadir, X. Li, S. V. Ambudkar, G. Szakacs, S. Akiyama, M. M. Gottesman, Human ABCB6 localizes to both the outer mitochondrial membrane and the plasma membrane. *Biochemistry* **46**, 9443–9452 (2007). doi:10.1021/bi700015m Medline

13. O. K. Vatamaniuk, E. A. Bucher, M. V. Sundaram, P. A. Rea, CeHMT-1, a putative phytochelatin transporter, is required for cadmium tolerance in *Caenorhabditis elegans*. *J. Biol. Chem.* **280**, 23684–23690 (2005). doi:10.1074/jbc.M503362200 Medline

14. S. Prévéral, L. Gayet, C. Moldes, J. Hoffmann, S. Mounicou, A. Gruet, F. Reynaud, R. Lobinski, J. M. Verbavatz, A. Vavasseur, C. Forestier, A common highly conserved cadmium detoxification mechanism from bacteria to humans: Heavy metal tolerance conferred by the ATP-binding cassette (ABC) transporter SpHMT1 requires glutathione but not metal-chelating phytochelatin peptides. *J. Biol. Chem.* **284**, 4936–4943 (2009). doi:10.1074/jbc.M808130200 Medline

15. T. Sooksa-Nguan, B. Yakubov, V. I. Kozlovskyy, C. M. Barkume, K. J. Howe, T. W. Thannhauser, M. A. Rutzke, J. J. Hart, L. V. Kochian, P. A. Rea, O. K. Vatamaniuk, *Drosophila* ABC transporter, DmHMT-1, confers tolerance to cadmium. DmHMT-1 and its yeast homolog, SpHMT-1, are not essential for vacuolar phytochelatin sequestration. *J. Biol. Chem.* **284**, 354–362 (2009). doi:10.1074/jbc.M806501200 Medline

16. G. Kuhnke, K. Neumann, U. Mühlenhoff, R. Lill, Stimulation of the ATPase activity of the yeast mitochondrial ABC transporter Atm1p by thiol compounds. *Mol. Membr. Biol.* **23**, 173–184 (2006). doi:10.1080/09687860500473630 Medline

17. A. Meister, Glutathione metabolism and its selective modification. *J. Biol. Chem.* **263**, 17205–17208 (1988). Medline

18. R. C. Fahey, A. R. Sundquist, Evolution of glutathione metabolism. *Adv. Enzymol.* **64**, 1–53 (1991). Medline

19. L. Masip, K. Veeravalli, G. Georgiou, The many faces of glutathione in bacteria. *Antioxid. Redox Signal.* **8**, 753–762 (2006). doi:10.1089/ars.2006.8.753 Medline

20. See supplementary materials on *Science* Online.

21. V. Srinivasan, A. J. Pierik, R. Lill, *Science* **343**, 1137 (2014).

22. R. J. Dawson, K. P. Locher, Structure of a bacterial multidrug ABC transporter. *Nature* **443**, 180–185 (2006). doi:10.1038/nature05155 Medline

23. S. G. Aller, J. Yu, A. Ward, Y. Weng, S. Chittaboina, R. Zhuo, P. M. Harrell, Y. T. Trinh, Q. Zhang, I. L. Urbatsch, G. Chang, Structure of P-glycoprotein reveals a molecular basis for poly-specific drug binding. *Science* **323**, 1718–1722 (2009). doi:10.1126/science.1168750 Medline

24. M. Hohl, C. Briand, M. G. Grütter, M. A. Seeger, Crystal structure of a heterodimeric ABC transporter in its inward-facing conformation. *Nat. Struct. Mol. Biol.* **19**, 395–402 (2012). doi:10.1038/nsmb.2267 Medline

25. M. S. Jin, M. L. Oldham, Q. Zhang, J. Chen, Crystal structure of the multidrug transporter P-glycoprotein from *Caenorhabditis elegans*. *Nature* **490**, 566–569 (2012). doi:10.1038/nature11448 Medline

26. C. A. Shintre, A. C. Pike, Q. Li, J. I. Kim, A. J. Barr, S. Goubin, L. Shrestha, J. Yang, G. Berridge, J. Ross, P. J. Stansfeld, M. S. Sansom, A. M. Edwards, C. Bountra, B. D. Marsden, F. von Delft, A. N. Bullock, O. Gileadi, N. A. Burgess-Brown, E. P. Carpenter, Structures of ABCB10, a human ATP-binding cassette transporter in apo- and nucleotide-bound states. *Proc. Natl. Acad. Sci. U.S.A.* **110**, 9710–9715 (2013). doi:10.1073/pnas.1217042110 Medline

27. A. Ward, C. L. Reyes, J. Yu, C. B. Roth, G. Chang, Flexibility in the ABC transporter MsbA: Alternating access with a twist. *Proc. Natl. Acad. Sci. U.S.A.* **104**, 19005–19010 (2007). doi:10.1073/pnas.0709388104 Medline

28. Z. E. Sauna, K. Nandigama, S. V. Ambudkar, Multidrug resistance protein 4 (ABCC4)-mediated ATP hydrolysis: Effect of transport substrates and characterization of the post-hydrolysis transition state. *J. Biol. Chem.* **279**, 48855–48864 (2004). doi:10.1074/jbc.M408849200 Medline

29. M. Herget, N. Kreissig, C. Kolbe, C. Schölz, R. Tampé, R. Abele, Purification and reconstitution of the antigen transport complex TAP: A prerequisite for determination of peptide stoichiometry and ATP hydrolysis. *J. Biol. Chem.* **284**, 33740–33749 (2009). doi:10.1074/jbc.M109.047779 Medline

30. G. Grass, B. Fan, B. P. Rosen, S. Franke, D. H. Nies, C. Rensing, ZitB (YbgR), a member of the cation diffusion facilitator family, is an additional zinc transporter in *Escherichia coli*. *J. Bacteriol.* **183**, 4664–4667 (2001). doi:10.1128/JB.183.15.4664-4667.2001 Medline

31. O. Lewinson, A. T. Lee, D. C. Rees, A P-type ATPase importer that discriminates between essential and toxic transition metals. *Proc. Natl. Acad. Sci. U.S.A.* **106**, 4677–4682 (2009). doi:10.1073/pnas.0900666106 Medline

32. M. S. Pittman, H. C. Robinson, R. K. Poole, A bacterial glutathione transporter (*Escherichia coli* CydDC) exports reductant to the periplasm. *J. Biol. Chem.* **280**, 32254–32261 (2005). doi:10.1074/jbc.M503075200 Medline

33. J. Li, K. F. Jaimes, S. G. Aller, Refined structures of mouse P-glycoprotein. *Protein Sci.* **23**, 34–46 (2014). doi:10.1002/pro.2387 Medline

34. E. Screpanti, C. Hunte, Discontinuous membrane helices in transport proteins and their correlation with function. *J. Struct. Biol.* **159**, 261–267 (2007). doi:10.1016/j.jsb.2007.01.011 Medline

35. W. Qi *et al.*, *J. Am. Chem. Soc.* **134**, 10754 (2012).

36. K. Hollenstein, R. J. P. Dawson, K. P. Locher, Structure and mechanism of ABC transporter proteins. *Curr. Opin. Struct. Biol.* **17**, 412–418 (2007). doi:10.1016/j.sbi.2007.07.003 Medline

37. J. F. Cotten, M. J. Welsh, Cystic fibrosis-associated mutations at arginine 347 alter the pore architecture of CFTR. Evidence for disruption of a salt bridge. *J. Biol. Chem.* **274**, 5429–5435 (1999). doi:10.1074/jbc.274.9.5429 Medline

38. G. Cui, C. S. Freeman, T. Knotts, C. Z. Prince, C. Kuang, N. A. McCarty, Two salt bridges differentially contribute to the maintenance of cystic fibrosis transmembrane conductance regulator (CFTR) channel function. *J. Biol. Chem.* **288**, 20758–20767 (2013). doi:10.1074/jbc.M113.476226 Medline

39. A. W. R. Serohijos, T. Hegedus, A. A. Aleksandrov, L. He, L. Cui, N. V. Dokholyan, J. R. Riordan, Phenylalanine-508 mediates a cytoplasmic-membrane domain contact in the CFTR 3D structure crucial to assembly and channel function. *Proc. Natl. Acad. Sci. U.S.A.* **105**, 3256–3261 (2008). doi:10.1073/pnas.0800254105 Medline

40. P. A. Karplus, K. Diederichs, Linking crystallographic model and data quality. *Science* **336**, 1030–1033 (2012). doi:10.1126/science.1218231 Medline

41. Q. Liu, Z. Zhang, W. A. Hendrickson, Multi-crystal anomalous diffraction for low-resolution macromolecular phasing. *Acta Crystallogr. D* **67**, 45–59 (2011). doi:10.1107/S0907444910046573 Medline

42. R. L. Tatusov, N. D. Fedorova, J. D. Jackson, A. R. Jacobs, B. Kiryutin, E. V. Koonin, D. M. Krylov, R. Mazumder, S. L. Mekhedov, A. N. Nikolskaya, B. S. Rao, S. Smirnov, A. V. Sverdlov, S. Vasudevan, Y. I. Wolf, J. J. Yin, D. A. Natale, The COG database: An updated version includes eukaryotes. *BMC Bioinformatics* **4**, 41 (2003). doi:10.1186/1471-2105-4-41 Medline

43. J. Lee, S. H. Kim, High-throughput T7 LIC vector for introducing C-terminal poly-histidine tags with variable lengths without extra sequences. *Protein Expr. Purif.* **63**, 58–61 (2009). doi:10.1016/j.pep.2008.09.005 Medline

44. F. W. Studier, Protein production by auto-induction in high density shaking cultures. *Protein Expr. Purif.* **41**, 207–234 (2005). doi:10.1016/j.pep.2005.01.016 Medline

45. J. Jancarik, S. H. Kim, Sparse matrix sampling: A screening method for crystallization of proteins. *J. Appl. Crystallogr.* **24**, 409–411 (1991). doi:10.1107/S0021889891004430

46. W. Kabsch, XDS. *Acta Crystallogr. D* **66**, 125–132 (2010). doi:10.1107/S0907444909047337 Medline

47. M. D. Winn, C. C. Ballard, K. D. Cowtan, E. J. Dodson, P. Emsley, P. R. Evans, R. M. Keegan, E. B. Krissinel, A. G. Leslie, A. McCoy, S. J. McNicholas, G. N. Murshudov, N. S. Pannu, E. A. Potterton, H. R. Powell, R. J. Read, A. Vagin, K. S. Wilson, Overview of the CCP4 suite and current developments. *Acta Crystallogr. D* **67**, 235–242 (2011). doi:10.1107/S0907444910045749 Medline

48. P. D. Adams, P. V. Afonine, G. Bunkóczi, V. B. Chen, N. Echols, J. J. Headd, L. W. Hung, S. Jain, G. J. Kapral, R. W. Grosse Kunstleve, A. J. McCoy, N. W. Moriarty, R. D. Oeffner, R. J. Read, D. C. Richardson, J. S. Richardson, T. C. Terwilliger, P. H. Zwart, The Phenix software for automated determination of macromolecular structures. *Methods* **55**, 94–106 (2011). doi:10.1016/j.ymeth.2011.07.005 Medline

49. P. Emsley, B. Lohkamp, W. G. Scott, K. Cowtan, Features and development of Coot. *Acta Crystallogr. D* **66**, 486–501 (2010). doi:10.1107/S0907444910007493 Medline

50. E. Krissinel, K. Henrick, Secondary-structure matching (SSM), a new tool for fast protein structure alignment in three dimensions. *Acta Crystallogr. D* **60**, 2256–2268 (2004). doi:10.1107/S0907444904026460 Medline

51. www.R-project.org (R Foundation for Statistical Computing, Vienna, 2012).

52. E. R. Geertsma, N. A. Nik Mahmood, G. K. Schuurman-Wolters, B. Poolman, Membrane reconstitution of ABC transporters and assays of translocator function. *Nat. Protoc.* **3**, 256–266 (2008). doi:10.1038/nprot.2007.519 Medline

53. T. P. Akerboom, H. Sies, Assay of glutathione, glutathione disulfide, and glutathione mixed disulfides in biological samples. *Methods Enzymol.* **77**, 373–382 (1981). doi:10.1016/S0076-6879(81)77050-2 Medline

54. J. Scherer, D. H. Nies, CzcP is a novel efflux system contributing to transition metal resistance in *Cupriavidus metallidurans* CH34. *Mol. Microbiol.* **73**, 601–621 (2009). doi:10.1111/j.1365-2958.2009.06792.x Medline

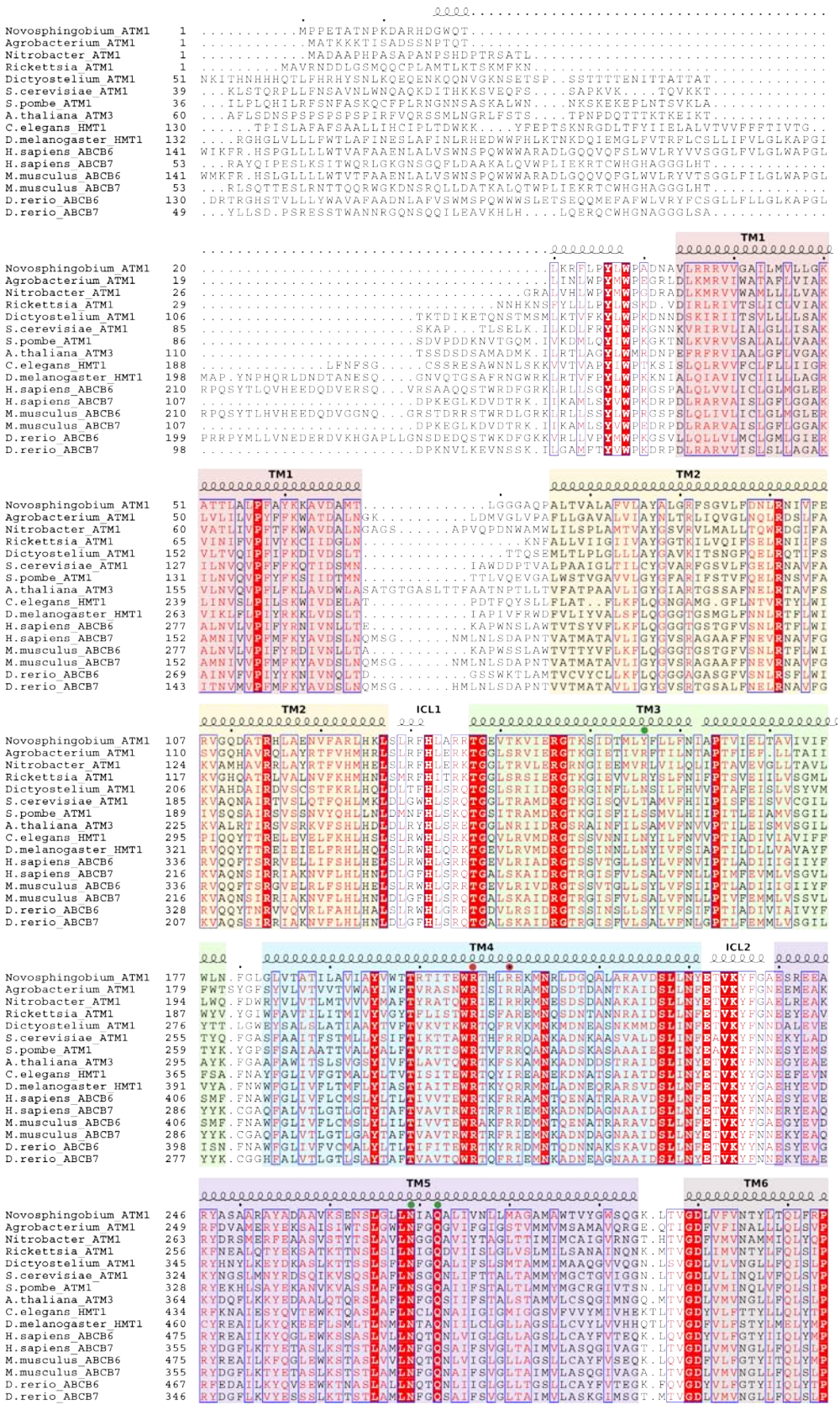
TM1
TM2
ICL1
TM3
TM4
ICL2
TM5
TM6
Novosphingobium_ATM1
Agrobacterium_ATM1
Nitrobacter_ATM1
Rickettsia_ATM1
Dictyostelium_ATM1
S.cerevisiae_ATM1
S.pombe_ATM1
A.thaliana_ATM3
C.elegans_HMT1
D.melanogaster_HMT1
H.sapiens_ABCB6
H.sapiens_ABCB7
M.musculus_ABCB6
M.musculus_ABCB7
D.rerio_ABCB6
D.rerio_ABCB7

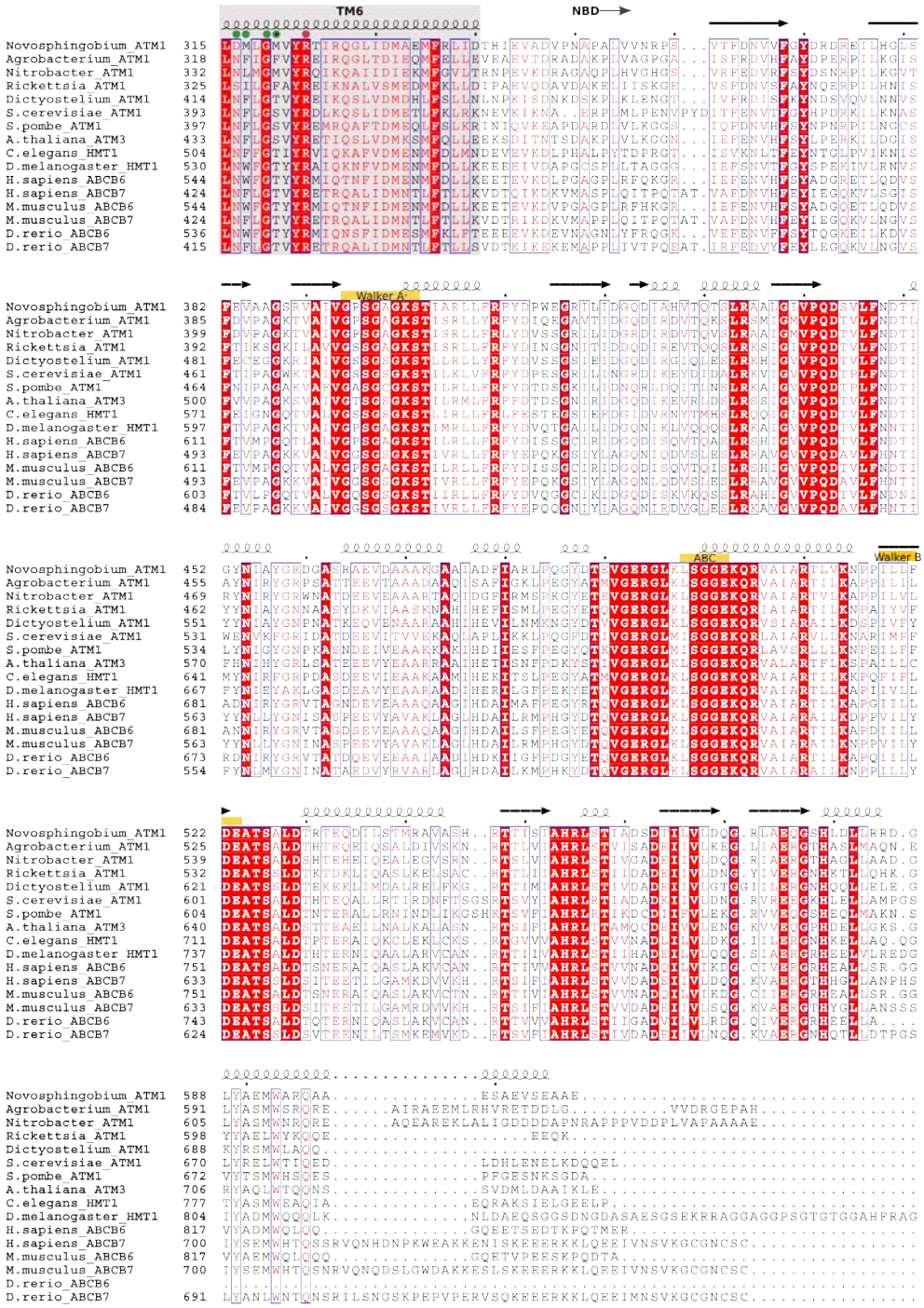


**Fig. S1**

CLUSTALW sequence alignment of Atm1/ABCB7/HMT1/ABCB6 from representative organisms from different kingdoms of life. Positions of the TMD helices and conserved ABC sequence motifs are indicated above the alignment. The key residues interacting with the primary GSSG binding sites are marked with green circles, while the residues interacting with the secondary GSSG binding sites are marked with red circles.

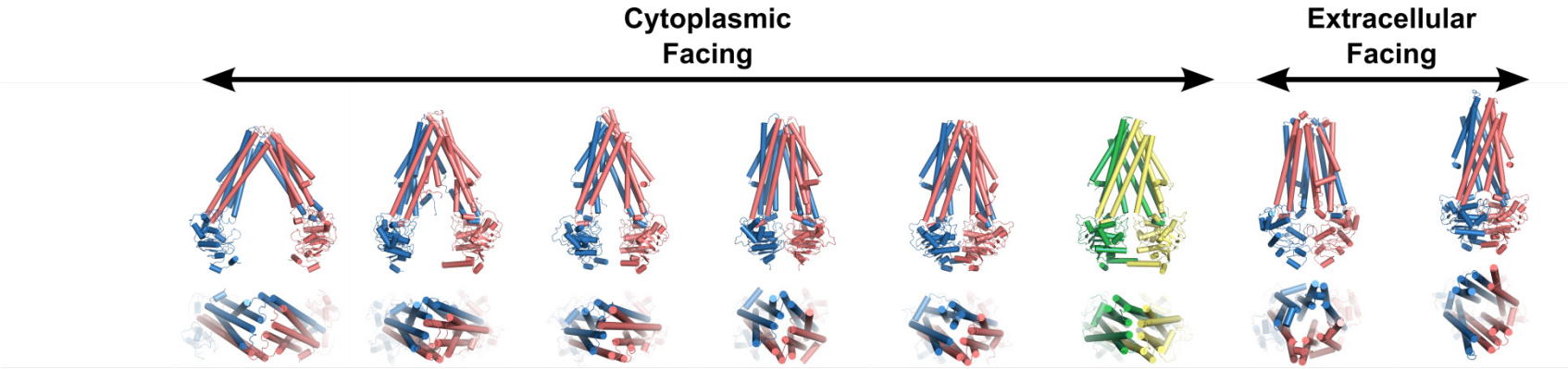


| Protein | *Ec* MsbA | *Ce* Pgp | *Mm* Pgp | *Hs* ABCB10 | *Tm* 287-288 | *Na* ATM1 | *Vc* MsbA | Sav1866 |
|---|---|---|---|---|---|---|---|---|
| **PDB ID** | 3B5W | 4F4C | 3G60 | 4AYT | 3QF4 | 4MRS | 3B5X | 2HYD |
| **Total Alignment RMSD (Å)** | 4.14 (547) | 4.97 (753) | 4.37 (1,027) | 3.63 (679) | 4.09 (962) | --- | 4.31 (628) | 3.81 (690) |
| **Subunit Alignment RMSD (Å)** | 3.65 (403) | 3.03/2.28 (467/422) | 3.26/3.26 (487/477) | 3.19 (436) | 3.38/3.88 (520/544) | --- | 3.4 (424) | 2.94 (418) |

**Fig. S2**

Comparison of representative ABC exporter structures ordered from inward (cytoplasmic) facing to outward (extracellular / periplasmic) facing. The upper structures are viewed along the membrane plane, while the lower structures are viewed from the extracellular side. *N. aromaticivorans* Atm1 is colored green-yellow. MsbA is the bacterial lipid flippase, and Pgp stands for P-glycoprotein. The structures are aligned with *Na* ATM1 as a reference, and the root-mean-square deviation (RMSD) distances are calculated with Coot Secondary Structure Matching (SSM) superposition. The values in parentheses are the number of aligned residues (~600 and ~1,200 total residues for the subunit and full alignment, respectively).

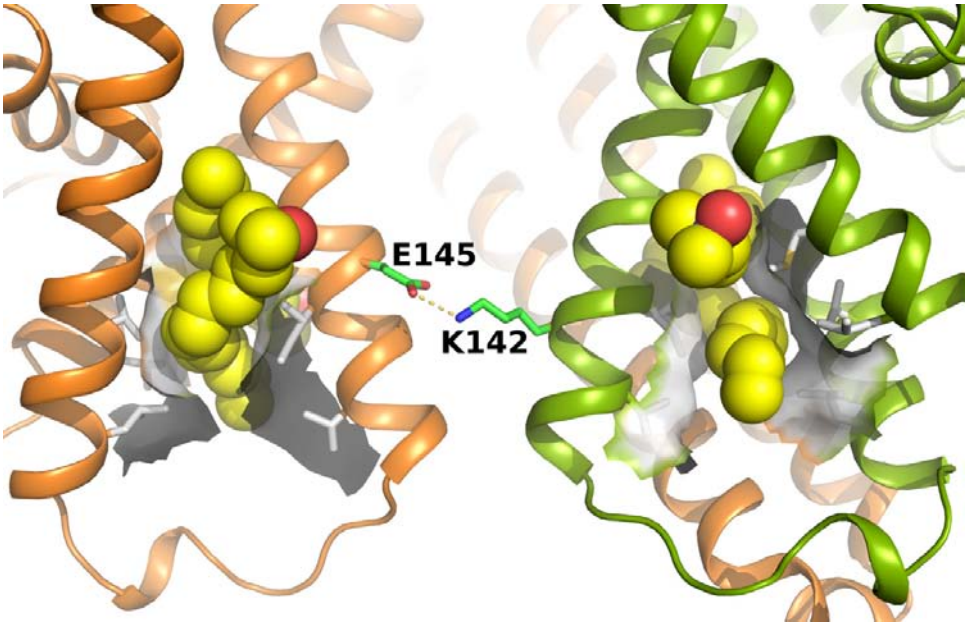


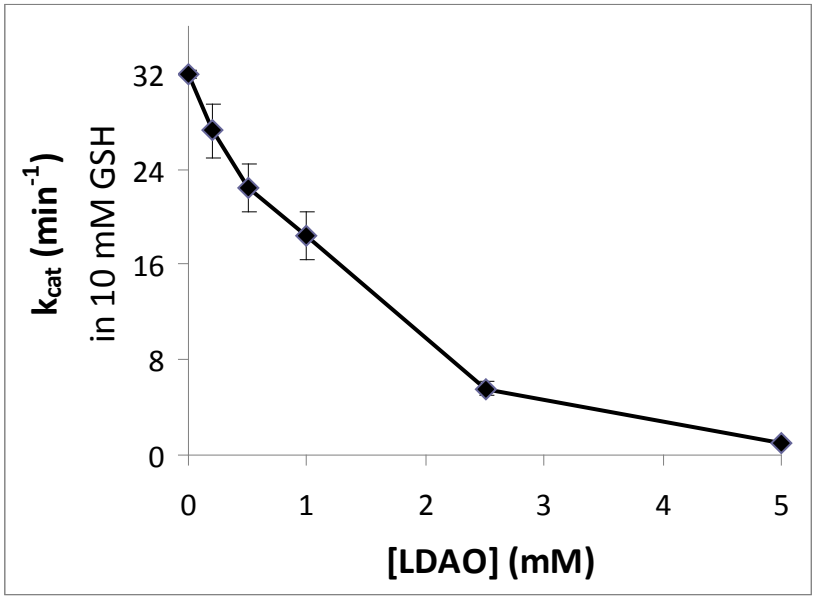


**Fig. S3**

Binding sites for LDAO, one of the critical crystallization detergents, in the TM2-ICL1-TM3 pocket and LDAO concentration dependent inhibition of the *Na*Atm1 ATPase activity. LDAO molecules (yellow carbon sphere models) are bound in the hydrophobic pocket (contoured in gray surfaces) formed between TM2-ICL1-TM3 and may stabilize ICL1 in an extended disordered conformation which to our knowledge has not been observed in other ABC exporter structures. This extension of ICL1 may prevent rearrangements of TM2 and TM3 during the transition to the ATPase competent outward facing conformation, thereby inhibiting the ATPase activity. The data points in the kinetic plot represent a mean value of N=3 with the error bars representing ± 1 S.D.

| Substrate | $k_{cat}$ / $K_m$ ($min^{-1}$ $mM^{-1}$) | $K_m$ (mM) | $k_{cat}$ ($min^{-1}$) |
|---|---|---|---|
| S-Ag GSH* | 2400 | 0.012 ± 0.001 | 29 ± 1 |
| S-Hg GSH* | 200 | 0.12 ± 0.04 | 24 ± 1 |
| S-DNB GSH | 120 | 0.21 ± 0.05 | 26 ± 2 |
| S-Hexyl GSH | 100 | 0.40 ± 0.12 | 40 ± 4 |
| S-Bimane GSH | 47 | 1.2 ± 0.2 | 56 ± 4 |
| GSSG | 29 | 0.97 ± 0.12 | 28 ± 1 |
| S-Methyl GSH | 7.9 | 3.9 ± 1.2 | 31 ± 3 |
| S-Lactoyl GSH | 4.7 | 10 ± 1 | 47 ± 2 |
| GSH | 3.8 | 15 ± 1 | 57 ± 2 |
| Glycine | 2.8 | 17 ± 3 | 47 ± 4 |
| γGlu-Cys | 2.6 | 10 ± 2 | 26 ± 2 |
| S-Sulfonic acid GSH | 2.6 | 12 ± 2 | 31 ± 2 |
| Ophthalmic acid | 1.7 | 36 ± 5 | 62 ± 6 |
| Cys-Gly | 0.13 | 46 ± 35 | 6.2 ± 3.2 |
| Sodium acetate | 0.13 | 10 ± 21 | 1.3 ± 1.2 |
| Sodium propionate | - | Not measurable | |

$v/[E]_T = k_{cat}[S] / (K_m + [S]) + k_{basal}$ where $k_{basal}$ = 8.8 ± 0.8 $min^{-1}$ in 1 mM ATP

* $K_m$ is reported as per mole of $Ag^+$ / $Hg^{2+}$ basis

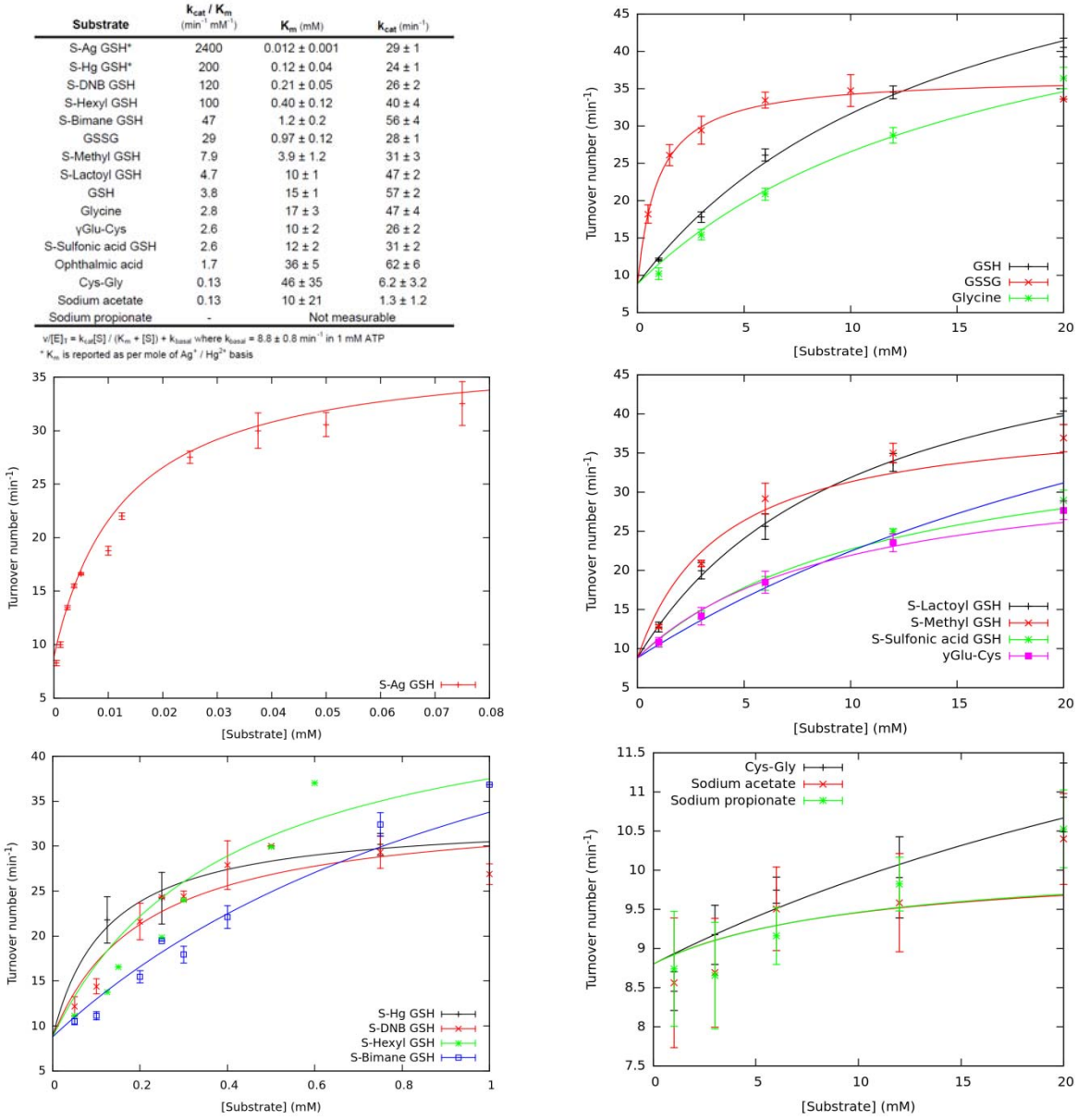


**Fig. S4**

Stimulation of the ATPase activity of *Na*Atm1 by glutathione derivatives. Each data point represents the average of N=3 independent measures (except S-Hexyl GSH : N=2) with the error bars representing ± 1 S.D.

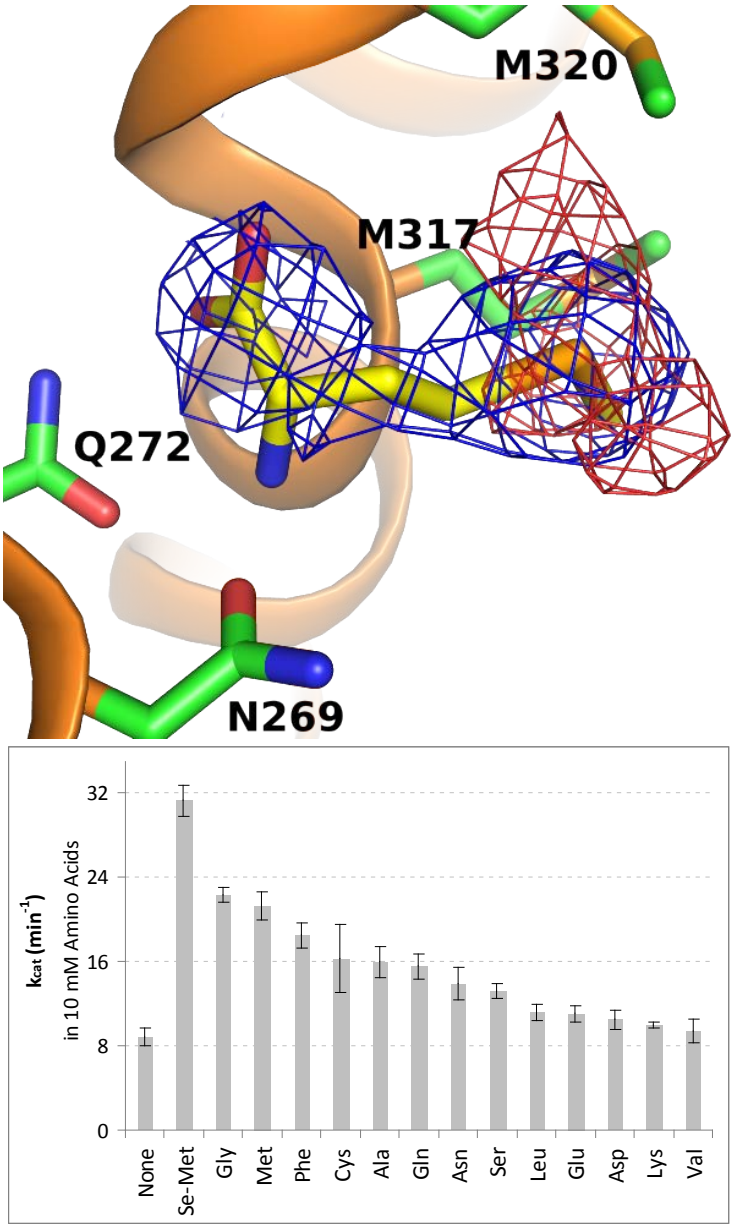


**Fig. S5**

Crystal structure of the binding of SeMet to *Na*Atm1, and stimulation of ATPase activity by 10 mM SeMet and other amino acids. The SeMet bound crystal structure indicates that the general binding model of amino acids follows the same motif as γ-Glu of GSH where primary interactions are made with the base functional groups of the amino acid. The blue mesh is 2Fo-Fc map contoured at 1.2σ, and the red mesh is Se-edge anomalous density map contoured at 3.5σ. The significant ATPase activities observed for SeMet and other amino acids indicates that the interactions of the α-amino and carboxyl groups with Asn 269 and Gln 272 are sufficient to stimulate ATPase activity. Each data point represents the average of N=3 independent measurements, with the error bars representing ± 1 S.D.

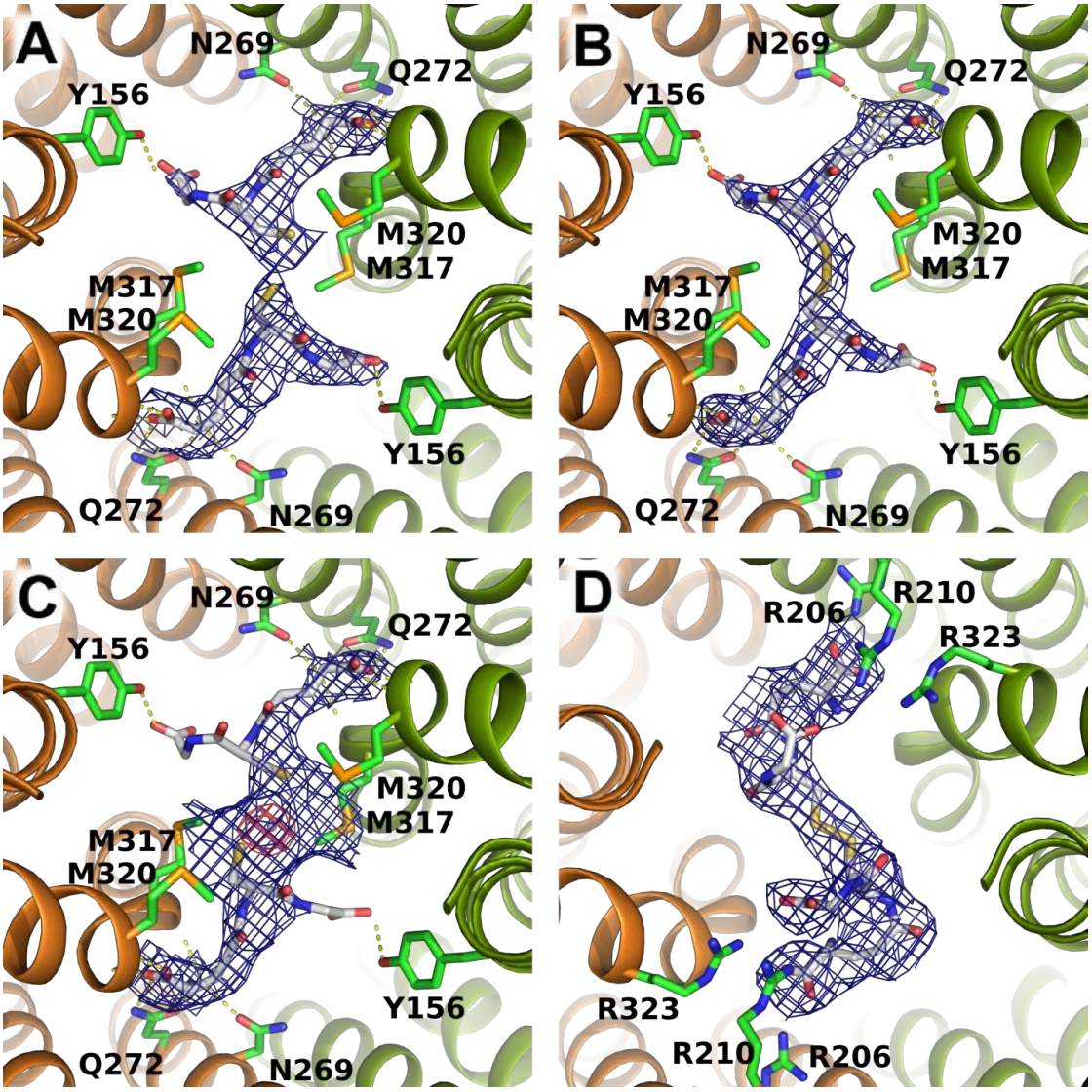


**Fig. S6**

Electron density maps of bound substrates. A) GSH bound structure, 2Fo-Fc map generated from Phenix.Refine contoured at 1.0σ. B) The primary GSSG binding site, 2Fo-Fc map contoured at 1.5σ. C) S-Hg $(GSH)_2$ 2Fo-Fc map contoured at 1.2σ (blue mesh), and Hg anomalous map contoured at 5σ (red mesh at center). D) The secondary GSSG binding site, 2Fo-Fc map contoured at 1.0σ**.** The electron density near chain (subunit) A (orange ribbon) is better defined than on the chain B side (green ribbon). In the primary binding site, the γ-Glu moiety of GSH is the best resolved part of the electron density map, while Gly is the least well defined, perhaps due to high flexibility. The secondary binding site can only be identified in the highest resolution GSSG bound structure, and the weaker density suggests more disorder or perhaps multiple overlapping binding sites. An alternative interpretation that the secondary binding site corresponds to detergent or other species is unlikely due to the shape of the density relative to that observed for LDAO and the absence of this feature in the apo-*Na*Atm1 structure.

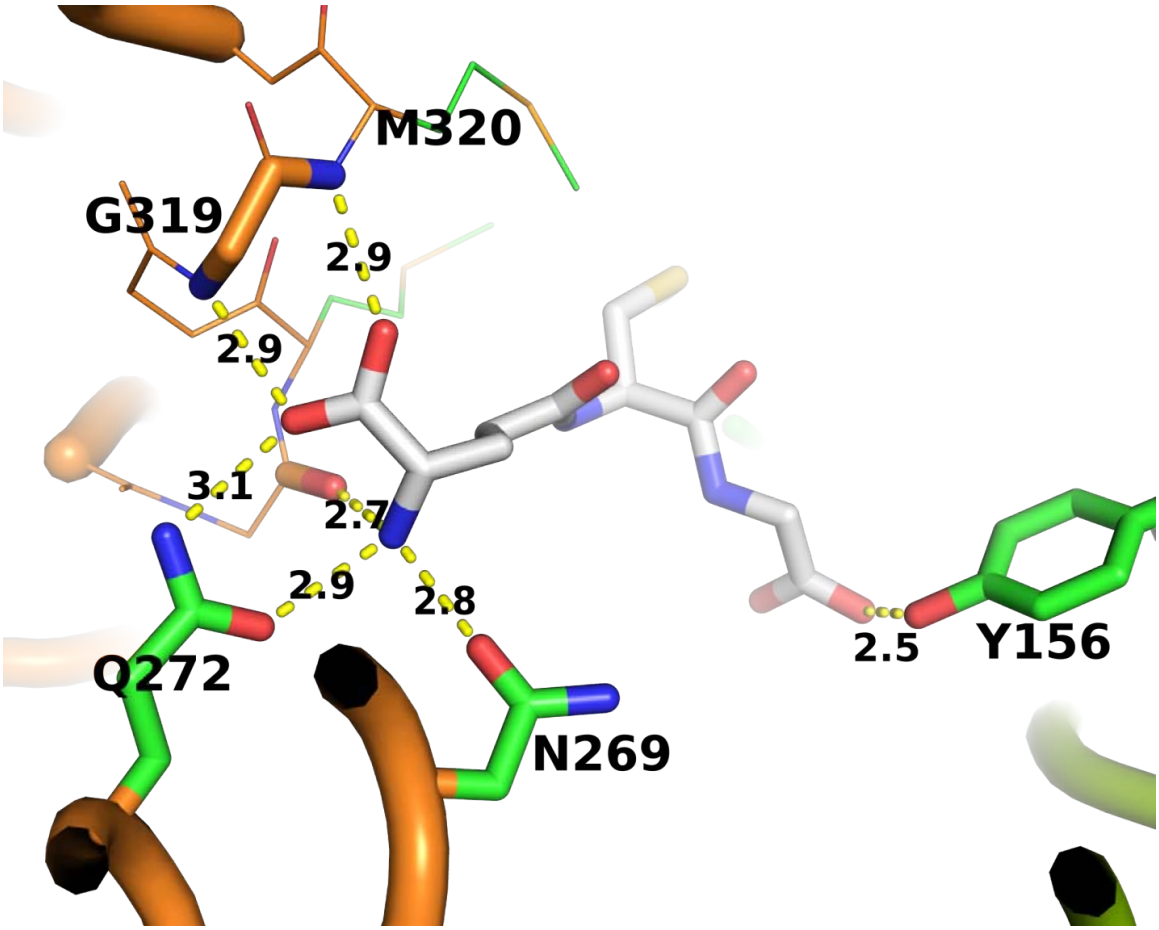


**Fig. S7**

Hydrogen bonding interaction map of GSSG. GSSG is modeled with light gray carbon atoms. The interacting backbone residue atoms are modeled as orange sticks. The interacting side chains are modeled as green carbon sticks. Hydrogen bonding distances are measured in Ångstroms, and averaged between homodimeric pairs.

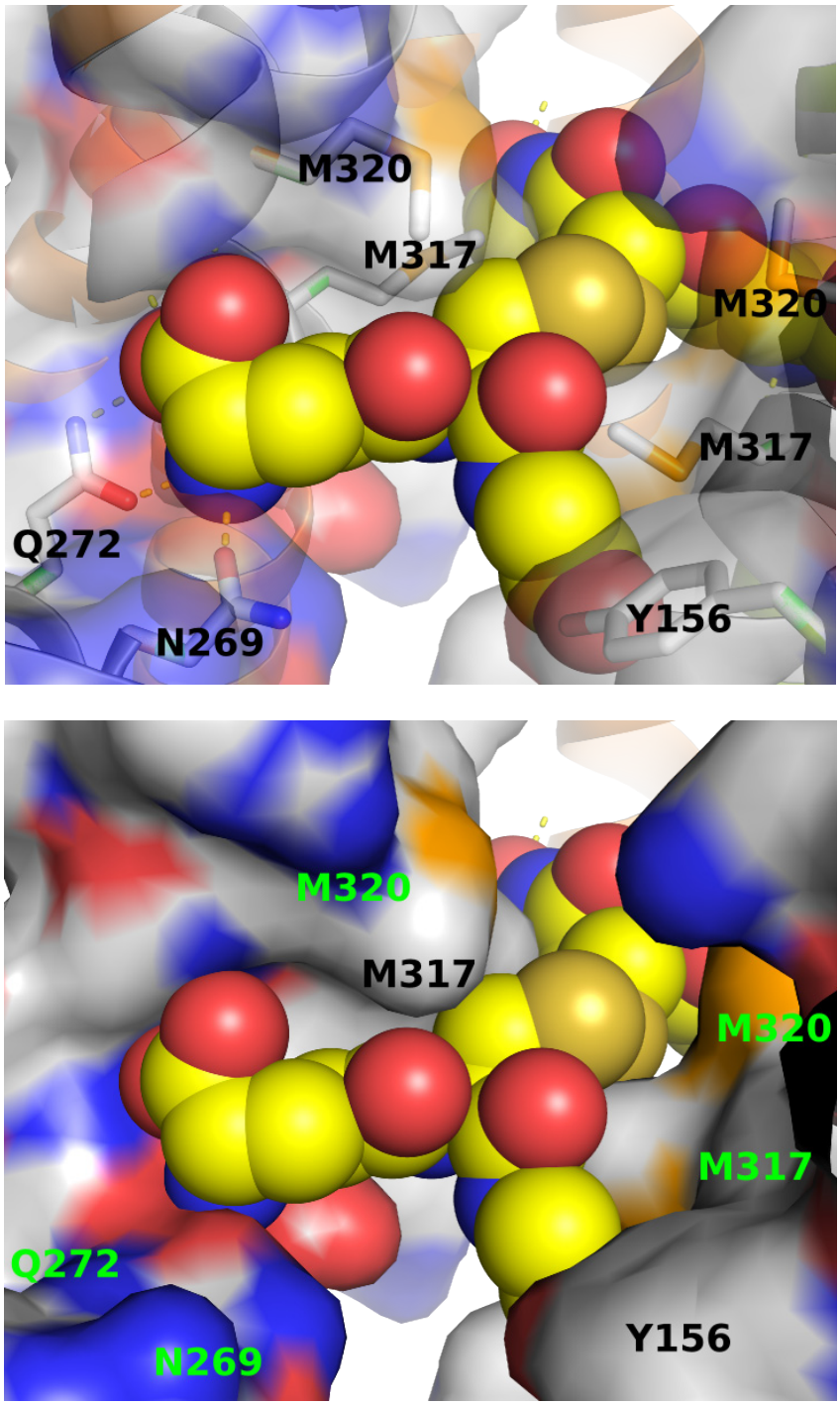


**Fig. S8**

Surface and sphere model of the primary GSSG binding site. Non-polar interactions are made by Leu 265 and Leu 268 (not shown for clarity) covering the γ-Glu moiety of GSH which contacts Asn 268 and Gln 272. Met 317/Met 320 from both *Na*Atm1 subunits make contacts along the GSH peptide backbone.

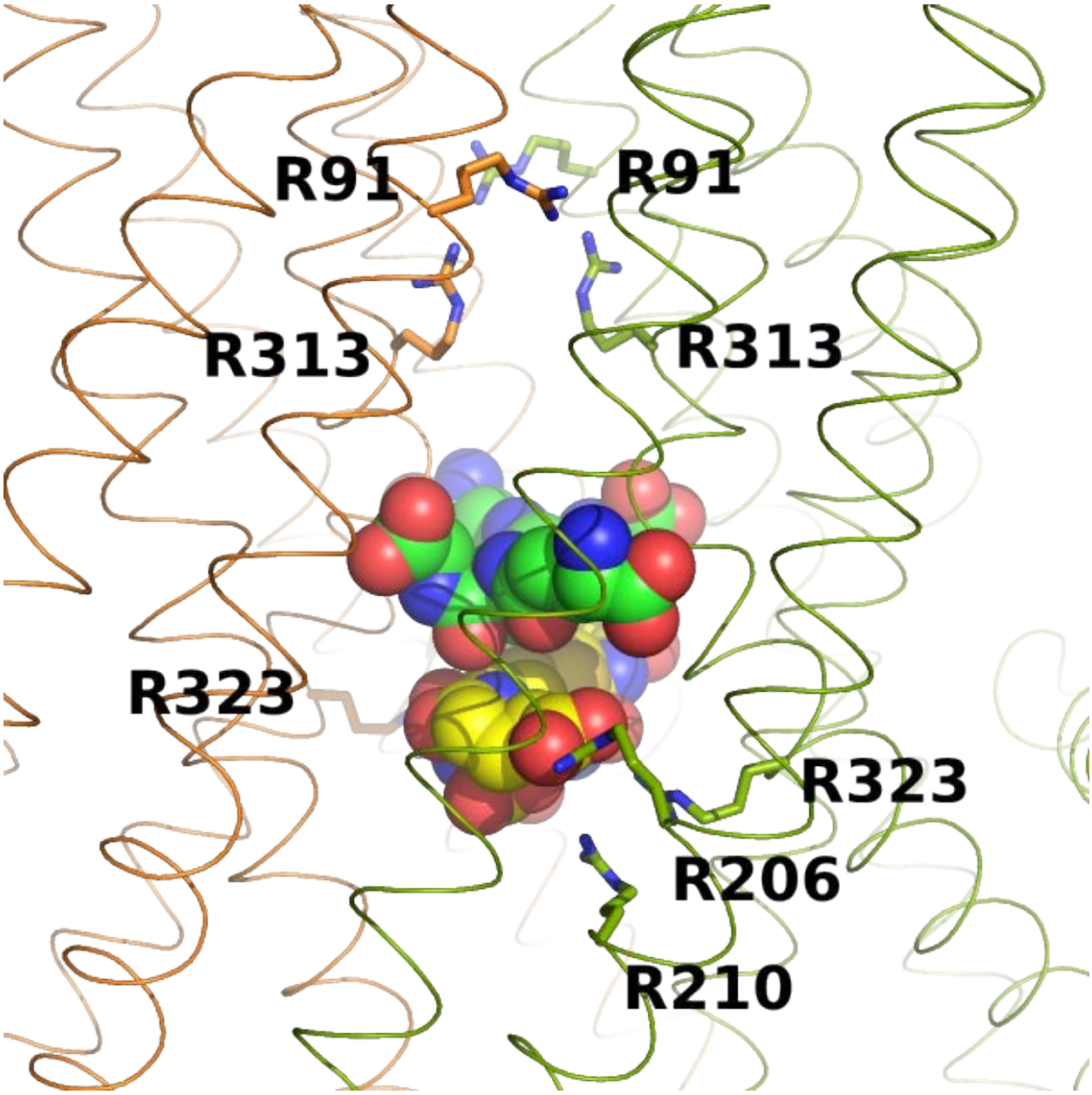


**Fig. S9**

Positioning of conserved Arg residues near GSH/GSSG binding sites. Highly conserved arginine residues 206, 210, and 323 are positioned near the cytoplasmic opening to the primary transmembrane binding site, while conserved arginine residues 91 and 313 are on the extracellular side of GSH/GSSG binding site. GSSG occupying the primary and secondary binding sites are modeled with green and yellow carbons, respectively.

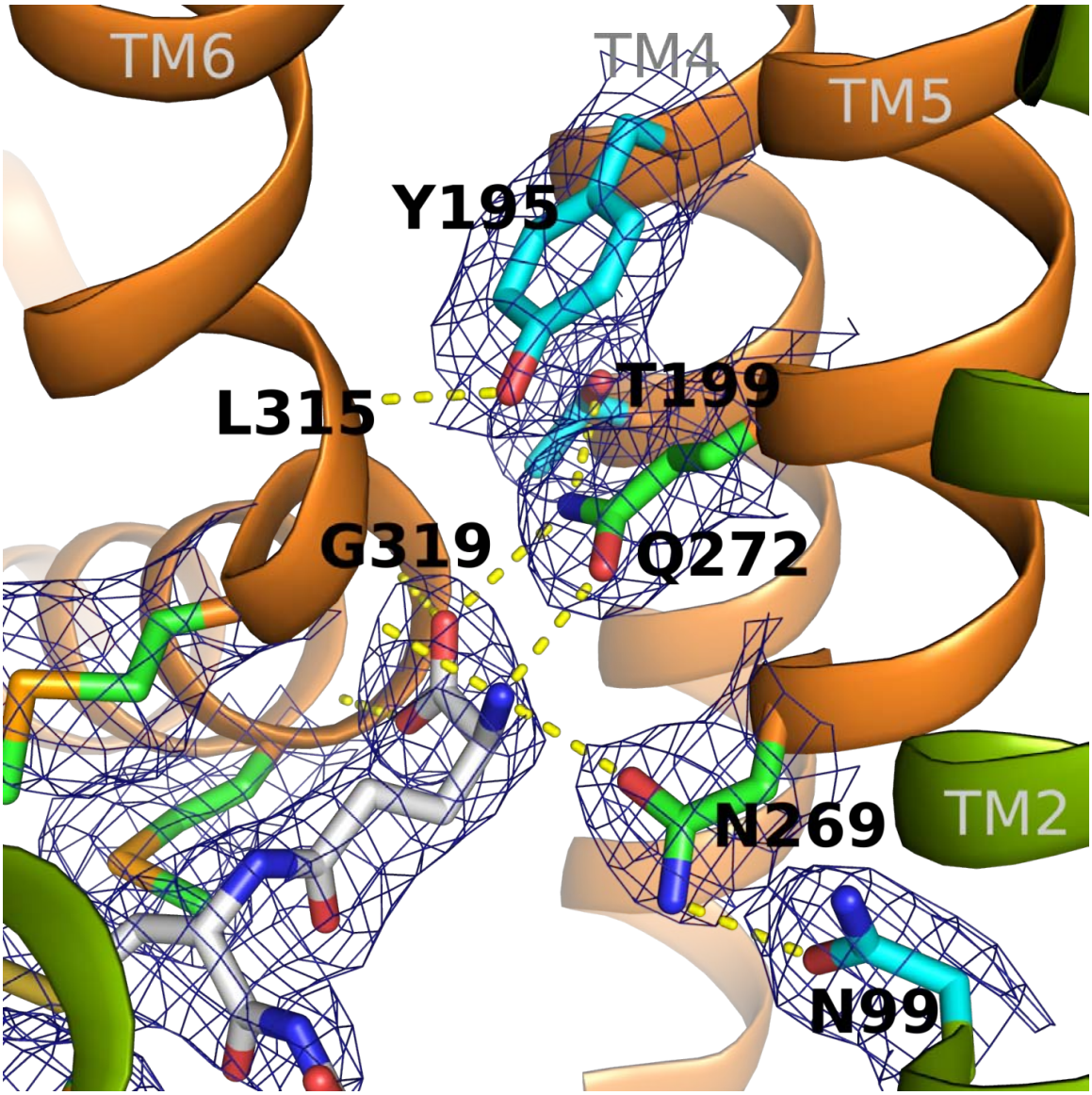


**Fig. S10**

Electron density map illustrating side chains of critical residues in the ligand binding site. Depicted is a 2.4 Å resolution 2Fo-Fc map for the GSSG-NaAtm1 complex generated with Phenix.Refine and contoured at 1.5σ. All residues and GSSG are clearly defined, illustrating the hydrogen bonding network with the γ-Glu moiety of GSSG. Carbons for GSSG, directly interacting protein side chains and non-ligand interacting residues are colored white, green and cyan, respectively.

**Table S1.**

Data collection and structure refinement summary.

**Data collection statistics** (Beamline : SSRL12-2; Detector: Pilatus 6M; Software: XDS, Aimless)

| Type | Apo-Se Inflection | Apo-Se Peak | GSH bound | GSSG bound | S-Hg GSH bound | SeMet bound |
|---|---|---|---|---|---|---|
| **PDB ID** | 4MRN | | 4MRP | 4MRS | 4MRV | 4MRR |
| **Space group** | C121 | | C121 | C121 | C121 | C121 |
| **Unit cell** | | | | | | |
| a, b, c (Å) | 322.8, 95.95, 81.13 | | 321.85, 95.26, 79.01 | 322.2, 95.4, 79.4 | 322.4, 95.62, 78.91 | 322.8, 95.95, 81.13 |
| α, β, γ (°) | 90, 101.8, 90 | | 90, 102, 90 | 90, 101.8, 90 | 90, 101.5, 90 | 90, 101.8, 90 |
| **Wavelength (Å)** | 0.9794 | 0.9792 | 0.9762 | 1.737 | 1.008 | 0.9686 |
| **Collection Angle / Oscillation (◦)** | 1200 / 0.2 | | 1080 / 0.3 | 1200 / 0.2 | 900 / 0.15 | 1080 / 0.2 |
| **Exposure (s) / Attenuation (%)** | 0.2 / 97 | | 0.3 / 95 | 0.2 / 97 | 0.2 / 97 | 0.2 / 94 |
| **Resolution (Å)** | 40-2.5 (2.55-2.50) | 40-2.65 (2.71-2.65) | 40-2.5 (2.55-2.5) | 40-2.345 (2.38-2.345) | 40-2.5 (2.55-2.5) | 40-2.97 (3.07-2.97) |
| **No. of unique reflections** | 80410 | 67666 | 79820 | 95204 | 80521 | 49540 |
| **Mean (I/sigmaI)** | 17.4 (0.5) | 14.9 (0.5) | 15.6 (0.6) | 16.2 (0.4) | 12.1 (0.5) | 18.4 (0.7) |
| **Completeness (%)** | 98.7 (99.2) | 98.7 (98.8) | 98.7 (99.3) | 96.1 (61.6) | 99 (99.6) | 98.6 (96.7) |
| **Average multiplicity** | 21 (21.5) | 21 (21) | 20.8 (21.3) | 19.8 (12.6) | 17.6 (17.9) | 20.9 (19.2) |
| **R-merge** (%)** | 15.9 (789) | 22.1 (856) | 18 (628) | 15.5 (657) | 22.7 (740) | 15.5 (516) |
| **$CC_{1/2}$ (%)** | 100 (19) | 100 (27) | 100 (38) | 100 (15) | 100 (15.3) | 100 (43) |

**Structure refinement statistics** (Software: Phenix.Refine)

| | | | | | |
|---|---|---|---|---|---|
| **Resolution (Å)** | 40-2.5 (2.54-2.5) | 40-2.5 (2.54-2.5) | 40-2.35 (2.39-2.35) | 40-2.5 (2.54-2.5) | 40-2.97 (3.02-2.97) |
| **Average B factor ($Å^2$)** | 65.8 | 65.9 | 63.7 | 60.2 | 64.1 |
| **$R_{work}/R_{free}$ (%)** | 20.0/22.7 | 20.2/23.1 | 19.0/22.1 | 20.6/23.4 | 20.3/23.6 |
| **CC* (%)** | 100 (54) | 100 (73) | 100 (58) | 100 (51) | 100 (55) |
| **$CC_{work}/CC_{free}$ (%)** | 91/93 (47/39) | 94/92 (60/57) | 94/93 (48/49) | 95/94 (47/29) | 92/94 (36/44) |
| **No. of atoms** | 9686 | 9673 | 9924 | 9734 | 9415 |
| Ligand | 94 | 124 | 230 | 125 | 112 |
| Solvent | 289 | 246 | 391 | 306 | 0 |
| **RMS deviations** | | | | | |
| Bond length (Å) | 0.009 | 0.009 | 0.009 | 0.01 | 0.011 |
| Bond angle (°) | 1.23 | 1.22 | 1.24 | 1.3 | 1.29 |
| **Ramachandran** | | | | | |
| Favored (%) | 98.2 | 98.1 | 98.5 | 98.2 | 97.0 |
| Outliers (%) | 0.17 | 0.08 | 0.08 | 0 | 0.08 |
| **Rotamer outliers (%)** | 0.64 | 0.64 | 0.43 | 1.1 | 1.4 |
| **Moprobity Clashscore** | 9.27 | 7.73 | 11.1 | 10.2 | 8.78 |

Values in parentheses are for the last resolution shell

** $R_{merge} = \Sigma_{hkl}\Sigma_i |I_i(hkl) - \langle I(hkl)\rangle| / \Sigma_{hkl}\Sigma_i I_i(hkl)$

**Table S2.**

CC* analysis of the refined structure against the unmerged intensities.

**Type** Apo

| Resolution Shell (Å) | CC* (%) | CC-work (%) | CC-free (%) | R-work (%) | R-free (%) |
|---|---|---|---|---|---|
| 39.8 - 6.78 | 100 | 86.8 | 88.6 | 18.7 | 20.2 |
| 6.77 - 5.38 | 100 | 92.3 | 91 | 19.1 | 20.2 |
| 5.38 - 4.7 | 100 | 95.7 | 92.1 | 15.3 | 16.8 |
| 4.7 - 4.27 | 100 | 96.2 | 96.5 | 14.6 | 16.2 |
| 4.27 - 3.97 | 100 | 95.1 | 89.5 | 16.9 | 22.3 |
| 3.97 - 3.73 | 99.9 | 94.1 | 94.5 | 17.7 | 20.3 |
| 3.73 - 3.55 | 99.9 | 94.3 | 89.9 | 18.1 | 23.1 |
| 3.55 - 3.39 | 99.6 | 92.6 | 89.9 | 19.7 | 24.7 |
| 3.39 - 3.26 | 99.2 | 92.4 | 83.7 | 21 | 25.6 |
| 3.26 - 3.15 | 98.8 | 91 | 86.4 | 22.9 | 27.6 |
| 3.15 - 3.05 | 97.8 | 90.2 | 86.3 | 23.6 | 29 |
| 3.05 - 2.96 | 96.2 | 87.8 | 84.8 | 24.9 | 27.8 |
| 2.96 - 2.89 | 94.6 | 86.1 | 81.6 | 27 | 30 |
| 2.89 - 2.82 | 90.1 | 81.1 | 62.9 | 29.7 | 35.6 |
| 2.82 - 2.75 | 87.4 | 79.3 | 57.7 | 30.8 | 38.4 |
| 2.75 - 2.69 | 83.3 | 74.7 | 68.7 | 32.7 | 32.1 |
| 2.69 - 2.64 | 81.1 | 70.5 | 56.3 | 35.1 | 36 |
| 2.64 - 2.59 | 74.2 | 60.4 | 69.9 | 38.9 | 39.5 |
| 2.59 - 2.54 | 67.6 | 58.8 | 44 | 39.6 | 44.4 |
| 2.54 - 2.5 | 53.6 | 46.6 | 38.7 | 41.7 | 42.5 |
| **Overall** | 100 | 91.2 | 92.6 | 20 | 22.7 |

**Type** GSH bound

| Resolution Shell (Å) | CC* (%) | CC-work (%) | CC-free (%) | R-work (%) | R-free (%) |
|---|---|---|---|---|---|
| 39.74 - 6.78 | 100 | 90.7 | 88.1 | 18.2 | 19.7 |
| 6.78 - 5.38 | 100 | 92.3 | 87.9 | 19.3 | 21.6 |
| 5.38 - 4.7 | 100 | 95.9 | 93.2 | 15.7 | 16.4 |
| 4.7 - 4.27 | 100 | 96.1 | 94.7 | 15.3 | 18.1 |
| 4.27 - 3.97 | 100 | 94.8 | 89.4 | 16.8 | 22.7 |
| 3.97 - 3.73 | 99.9 | 94.9 | 96.7 | 16.6 | 19.3 |
| 3.73 - 3.55 | 99.9 | 94.7 | 90.9 | 18.1 | 23 |
| 3.55 - 3.39 | 99.7 | 92.6 | 89.6 | 20.3 | 23.6 |
| 3.39 - 3.26 | 99.5 | 91.6 | 79.3 | 21.4 | 26.7 |
| 3.26 - 3.15 | 99.1 | 89 | 84.1 | 23.9 | 25.6 |
| 3.15 - 3.05 | 98.6 | 91 | 84.1 | 25.2 | 31.5 |
| 3.05 - 2.96 | 97.7 | 89.3 | 80.3 | 25.6 | 29.7 |
| 2.96 - 2.89 | 96.7 | 88.6 | 82.6 | 26.1 | 28.4 |
| 2.89 - 2.82 | 94.8 | 85.4 | 69.7 | 28.4 | 35.4 |
| 2.82 - 2.75 | 92.4 | 81.9 | 70.4 | 29.9 | 34.6 |
| 2.75 - 2.69 | 90 | 81.9 | 78.8 | 30.3 | 32.9 |
| 2.69 - 2.64 | 88.7 | 78.4 | 70.1 | 33.6 | 36.4 |
| 2.64 - 2.59 | 85.2 | 75.2 | 60.5 | 36.6 | 38.5 |
| 2.59 - 2.54 | 80.5 | 70.7 | 60.8 | 40 | 44.9 |
| 2.54 - 2.5 | 72.5 | 59.8 | 57.2 | 45.4 | 44.7 |
| **Overall** | 100 | 93.9 | 91.8 | 20.2 | 23.1 |

**Type** GSSG bound

| Resolution Shell (Å) | CC* (%) | CC-work (%) | CC-free (%) | R-work (%) | R-free (%) |
|---|---|---|---|---|---|
| 39.42 - 6.37 | 100 | 91.4 | 89.8 | 17.8 | 18.3 |
| 6.37 - 5.06 | 100 | 94 | 92.3 | 18 | 20.4 |
| 5.06 - 4.42 | 100 | 95.3 | 95 | 15 | 16.5 |
| 4.42 - 4.02 | 100 | 94.9 | 92.2 | 15.5 | 20 |
| 4.02 - 3.73 | 100 | 94.5 | 94 | 16.3 | 19.5 |
| 3.73 - 3.51 | 99.9 | 94.5 | 91.6 | 17.2 | 21.5 |
| 3.51 - 3.33 | 99.8 | 92.5 | 87.2 | 19 | 22.7 |
| 3.33 - 3.19 | 99.6 | 91.7 | 85 | 19.4 | 23.6 |
| 3.19 - 3.07 | 99.4 | 92.6 | 86 | 20.4 | 25.2 |
| 3.07 - 2.96 | 98.8 | 91.1 | 84.9 | 21.4 | 25.9 |
| 2.96 - 2.87 | 98.2 | 90.6 | 88.7 | 22 | 27.5 |
| 2.87 - 2.79 | 97.1 | 89.8 | 77.8 | 22.6 | 28.2 |
| 2.79 - 2.71 | 96.1 | 88.9 | 81.7 | 24 | 28.5 |
| 2.71 - 2.65 | 93.4 | 85.4 | 68.6 | 25.7 | 30.9 |
| 2.65 - 2.59 | 92 | 83.9 | 78.5 | 27.2 | 31.5 |
| 2.59 - 2.53 | 88.8 | 80.5 | 71.7 | 28.2 | 33.3 |
| 2.53 - 2.48 | 82.7 | 73.6 | 66.7 | 30.4 | 34.3 |
| 2.48 - 2.43 | 79.2 | 69.2 | 61.1 | 32.3 | 36 |
| 2.43 - 2.39 | 68.7 | 59 | 55 | 34.7 | 38.7 |
| 2.39 - 2.35 | 58.3 | 48.2 | 48.7 | 37.9 | 37.7 |
| **Overall** | 100 | 94.1 | 93.4 | 19 | 22 |

**Type** S-Hg GSH bound

| Resolution Shell (Å) | CC* (%) | CC-work (%) | CC-free (%) | R-work (%) | R-free (%) |
|---|---|---|---|---|---|
| 39.49 - 6.78 | 100 | 93 | 91.4 | 18 | 19.1 |
| 6.77 - 5.38 | 100 | 92.1 | 88.9 | 19.4 | 21.1 |
| 5.38 - 4.7 | 100 | 94.4 | 91.1 | 16.9 | 19.4 |
| 4.7 - 4.27 | 100 | 95.4 | 94.9 | 15.8 | 18.9 |
| 4.27 - 3.97 | 99.9 | 94.3 | 92.7 | 16.7 | 20 |
| 3.97 - 3.73 | 99.9 | 94.2 | 92 | 17 | 19 |
| 3.73 - 3.55 | 99.8 | 94.1 | 90.7 | 18.7 | 23.8 |
| 3.55 - 3.39 | 99.4 | 92 | 89.3 | 20.9 | 22.6 |
| 3.39 - 3.26 | 99 | 90.9 | 80.4 | 21.3 | 27.9 |
| 3.26 - 3.15 | 98.2 | 89.7 | 86.3 | 23 | 25.4 |
| 3.15 - 3.05 | 96.9 | 88.9 | 87.1 | 24.1 | 29.9 |
| 3.05 - 2.96 | 94.9 | 85.6 | 80.1 | 26.9 | 30.5 |
| 2.96 - 2.89 | 92.4 | 82.1 | 77.7 | 29.5 | 33.9 |
| 2.89 - 2.82 | 88.1 | 78 | 68.1 | 29.5 | 34.9 |
| 2.82 - 2.75 | 86.1 | 77.4 | 60 | 30.9 | 36.5 |
| 2.75 - 2.69 | 80.4 | 71.7 | 67.9 | 31.8 | 33.2 |
| 2.69 - 2.64 | 77.4 | 68.1 | 56.5 | 32.8 | 36.5 |
| 2.64 - 2.59 | 72.2 | 61.2 | 64.8 | 35.8 | 40.9 |
| 2.59 - 2.54 | 63.2 | 54.5 | 51.3 | 37 | 36.9 |
| 2.54 - 2.5 | 51.4 | 46.9 | 28.6 | 42 | 42.8 |
| **Overall** | 100 | 95.2 | 93.9 | 20.6 | 23.4 |

**Type** Se-Met bound

| Resolution Shell (Å) | CC* (%) | CC-work (%) | CC-free (%) | R-work (%) | R-free (%) |
|---|---|---|---|---|---|
| 39.5 - 8.04 | 100 | 87.8 | 92.6 | 18.8 | 19.6 |
| 8.04 - 6.39 | 100 | 94.1 | 92.9 | 18.3 | 20.7 |
| 6.39 - 5.59 | 100 | 91.5 | 87.2 | 20.5 | 22.8 |
| 5.59 - 5.08 | 100 | 95.3 | 94.6 | 17.5 | 21.9 |
| 5.08 - 4.71 | 100 | 95.9 | 90.7 | 15.2 | 20.2 |
| 4.71 - 4.44 | 100 | 96.3 | 96.4 | 15.5 | 20 |
| 4.43 - 4.21 | 100 | 96 | 90.9 | 17.1 | 18.7 |
| 4.21 - 4.03 | 99.9 | 95.1 | 94.6 | 18 | 21.6 |
| 4.03 - 3.88 | 99.8 | 94.9 | 89.5 | 18.9 | 24 |
| 3.88 - 3.74 | 99.7 | 94.2 | 88.7 | 19.5 | 26.3 |
| 3.74 - 3.62 | 99.5 | 94.1 | 93.9 | 20.3 | 27.6 |
| 3.62 - 3.52 | 99.1 | 93.3 | 85.7 | 22.1 | 29.1 |
| 3.52 - 3.43 | 97.8 | 87.5 | 65.8 | 27 | 33.7 |
| 3.43 - 3.34 | 97.2 | 89.9 | 86.2 | 27.7 | 29.8 |
| 3.34 - 3.27 | 95.8 | 85.7 | 74.8 | 28.5 | 35.6 |
| 3.27 - 3.2 | 93.7 | 83.1 | 69.3 | 31.1 | 36.1 |
| 3.2 - 3.14 | 90.4 | 80.4 | 62 | 32 | 40.9 |
| 3.14 - 3.08 | 87.1 | 74.5 | 69.9 | 36.2 | 39.5 |
| 3.08 - 3.02 | 80.3 | 61.8 | 51.1 | 43.5 | 43.4 |
| 3.02 - 2.97 | 74.3 | 59.7 | 37.5 | 52 | 54.4 |
| **Overall** | 100 | 91.9 | 94.7 | 20.3 | 23.6 |

**Table S3.**

Detailed data processing statistics.

| Type | Apo – SeMet Inflection | | | | | | | |
|---|---|---|---|---|---|---|---|---|
| Resolution Shell (Å) | Total Reflection | Unique Reflection | Multiplicity | Mean (I/sigI) | Completeness (%) | Rmerge (%) | CC1/2 (%) | CC1/2 pairs |
| 40 - 12.75 | 12292 | 621 | 19.8 | 130.9 | 94.1 | 2.1 | 100 | 621 |
| 12.75 - 9.02 | 22672 | 1140 | 19.9 | 120.7 | 98.8 | 2.2 | 100 | 1140 |
| 9.02 - 7.36 | 31509 | 1484 | 21.2 | 94.2 | 99.8 | 2.8 | 100 | 1484 |
| 7.36 - 6.38 | 34036 | 1711 | 19.9 | 60.2 | 97.3 | 4.4 | 99.9 | 1709 |
| 6.38 - 5.7 | 40489 | 1940 | 20.9 | 48.4 | 98.6 | 5.8 | 99.9 | 1940 |
| 5.7 - 5.21 | 46410 | 2176 | 21.3 | 45.5 | 99.7 | 6.3 | 99.9 | 2176 |
| 5.21 - 4.82 | 51329 | 2360 | 21.7 | 50.5 | 99.5 | 5.5 | 100 | 2360 |
| 4.82 - 4.51 | 52559 | 2499 | 21 | 46.2 | 98.5 | 6.1 | 100 | 2498 |
| 4.51 - 4.25 | 52417 | 2616 | 20 | 38.6 | 97.1 | 7.4 | 99.9 | 2613 |
| 4.25 - 4.03 | 59805 | 2816 | 21.2 | 29.8 | 99.2 | 10.4 | 99.9 | 2815 |
| 4.03 - 3.84 | 63905 | 2978 | 21.5 | 24.5 | 99.1 | 13 | 99.8 | 2978 |
| 3.84 - 3.68 | 66766 | 3099 | 21.5 | 19.2 | 99.5 | 17.6 | 99.6 | 3099 |
| 3.68 - 3.54 | 70234 | 3253 | 21.6 | 13.9 | 99.5 | 25.4 | 99.4 | 3253 |
| 3.54 - 3.41 | 65789 | 3290 | 20 | 9.3 | 97.4 | 37.1 | 98 | 3287 |
| 3.41 - 3.29 | 69420 | 3404 | 20.4 | 7.6 | 98.2 | 47.4 | 97.4 | 3401 |
| 3.29 - 3.19 | 74797 | 3558 | 21 | 5.8 | 98.6 | 63.7 | 95.9 | 3557 |
| 3.19 - 3.09 | 78483 | 3710 | 21.2 | 4.2 | 98.9 | 89.7 | 92.5 | 3708 |
| 3.09 - 3 | 82664 | 3855 | 21.4 | 3.2 | 99.3 | 116.7 | 88.1 | 3855 |
| 3 - 2.92 | 84509 | 3922 | 21.5 | 2.6 | 99 | 144.8 | 83.4 | 3921 |
| 2.92 - 2.85 | 87165 | 4022 | 21.7 | 1.9 | 99.6 | 195.6 | 76.9 | 4022 |
| 2.85 - 2.78 | 80815 | 4037 | 20 | 1.3 | 97.2 | 270.9 | 61.1 | 4032 |
| 2.78 - 2.72 | 84985 | 4179 | 20.3 | 1.2 | 98.1 | 301.5 | 61.6 | 4177 |
| 2.72 - 2.66 | 88144 | 4238 | 20.8 | 0.9 | 98.8 | 394.2 | 50.5 | 4237 |
| 2.66 - 2.6 | 94416 | 4459 | 21.2 | 0.7 | 98.9 | 504.5 | 39.1 | 4457 |
| 2.6 - 2.55 | 95172 | 4469 | 21.3 | 0.6 | 98.8 | 622.7 | 33.6 | 4468 |
| 2.55 - 2.5 | 98135 | 4574 | 21.5 | 0.5 | 99.2 | 788.5 | 19 | 4570 |
| 40 -2.5 | 1688917 | 80410 | 21 | 17.4 | 98.7 | 15.9 | 100 | 80378 |

| Type | GSSG Bound | | | | | | | |
|---|---|---|---|---|---|---|---|---|
| Resolution Shell (Å) | Total Reflection | Unique Reflection | Multiplicity | Mean (I/sigI) | Completeness (%) | Rmerge (%) | CC1/2 (%) | CC1/2 pairs |
| 40 - 12.82 | 12225 | 629 | 19.4 | 96.9 | 96.6 | 2.9 | 100 | 629 |
| 12.82 - 9.07 | 20167 | 1093 | 18.5 | 90.7 | 96.2 | 2.7 | 100 | 1093 |
| 9.07 - 7.4 | 28779 | 1443 | 19.9 | 75.5 | 99.1 | 3.3 | 100 | 1443 |
| 7.4 - 6.41 | 35220 | 1729 | 20.4 | 53.6 | 99.4 | 4.8 | 100 | 1729 |
| 6.41 - 5.74 | 36489 | 1864 | 19.6 | 44.4 | 96.9 | 5.8 | 99.9 | 1864 |
| 5.74 - 5.24 | 40745 | 2111 | 19.3 | 42.9 | 98.5 | 6.2 | 99.9 | 2111 |
| 5.24 - 4.85 | 47267 | 2314 | 20.4 | 51.6 | 99.2 | 5.1 | 100 | 2310 |
| 4.85 - 4.53 | 51506 | 2476 | 20.8 | 50.6 | 99.6 | 5.4 | 100 | 2476 |
| 4.53 - 4.27 | 55477 | 2643 | 21 | 46.5 | 99.7 | 6 | 99.9 | 2643 |
| 4.27 - 4.06 | 55711 | 2762 | 20.2 | 38.5 | 98.3 | 7.4 | 99.9 | 2761 |
| 4.06 - 3.87 | 55344 | 2836 | 19.5 | 32.2 | 97 | 9 | 99.9 | 2831 |
| 3.87 - 3.7 | 62581 | 3046 | 20.5 | 27.6 | 99.2 | 10.9 | 99.8 | 3043 |
| 3.7 - 3.56 | 66696 | 3182 | 21 | 21.5 | 99.2 | 14.8 | 99.7 | 3180 |
| 3.56 - 3.43 | 68946 | 3295 | 20.9 | 16.3 | 99.2 | 20.5 | 99.4 | 3292 |
| 3.43 - 3.31 | 72202 | 3403 | 21.2 | 13.6 | 98.7 | 25 | 99.3 | 3399 |
| 3.31 - 3.21 | 71310 | 3505 | 20.3 | 10.7 | 98.1 | 31.7 | 98.6 | 3504 |
| 3.21 - 3.11 | 68832 | 3560 | 19.3 | 7.7 | 97.4 | 44.3 | 97.7 | 3551 |
| 3.11 - 3.02 | 74387 | 3690 | 20.2 | 6.2 | 98.2 | 56.5 | 96.5 | 3679 |
| 3.02 - 2.94 | 77811 | 3805 | 20.4 | 5 | 98.4 | 72.8 | 95.1 | 3797 |
| 2.94 - 2.86 | 81648 | 3966 | 20.6 | 4.1 | 98.7 | 88.3 | 93.3 | 3964 |
| 2.86 - 2.8 | 83521 | 4035 | 20.7 | 3.2 | 99.1 | 112.7 | 89 | 4032 |
| 2.8 - 2.73 | 85051 | 4109 | 20.7 | 2.8 | 98.7 | 126.6 | 88.3 | 4099 |
| 2.73 - 2.67 | 77197 | 4180 | 18.5 | 1.9 | 97.1 | 173.3 | 78.3 | 4169 |
| 2.67 - 2.62 | 84582 | 4270 | 19.8 | 1.7 | 97.9 | 206.9 | 75.6 | 4257 |
| 2.62 - 2.56 | 87292 | 4345 | 20.1 | 1.5 | 98 | 233.6 | 71.7 | 4335 |
| 2.56 - 2.51 | 90145 | 4465 | 20.2 | 1.1 | 98.1 | 303.2 | 58.1 | 4461 |
| 2.51 - 2.47 | 91769 | 4528 | 20.3 | 1 | 97.1 | 349.3 | 50.1 | 4526 |
| 2.47 - 2.42 | 90975 | 4552 | 20 | 0.8 | 96.3 | 400.3 | 44.5 | 4539 |
| 2.42 - 2.38 | 74207 | 4373 | 17 | 0.6 | 91.7 | 501.2 | 29.4 | 4348 |
| 2.38 - 2.34 | 37675 | 2995 | 12.6 | 0.4 | 61.6 | 657.1 | 15 | 2892 |
| 40-2.34 | 1885757 | 95204 | 19.8 | 16.2 | 96.1 | 15.5 | 99.9 | 94957 |

| Type | GSH bound | | | | | | | |
|---|---|---|---|---|---|---|---|---|
| Resolution Shell (Å) | Total Reflection | Unique Reflection | Multiplicity | Mean (I/sigI) | Completeness (%) | Rmerge (%) | CC1/2 (%) | CC1/2 pairs |
| 40 - 12.75 | 11718 | 617 | 19 | 100 | 94.5 | 2.6 | 100 | 617 |
| 12.75 - 9.02 | 21555 | 1130 | 19.1 | 94 | 98.4 | 2.7 | 100 | 1129 |
| 9.02 - 7.36 | 30066 | 1464 | 20.5 | 73.2 | 99.5 | 3.5 | 100 | 1464 |
| 7.36 - 6.38 | 33117 | 1697 | 19.5 | 47.1 | 97.5 | 5.4 | 99.9 | 1695 |
| 6.38 - 5.7 | 39170 | 1927 | 20.3 | 38.5 | 98.6 | 7.1 | 99.9 | 1926 |
| 5.7 - 5.21 | 45395 | 2168 | 20.9 | 38.4 | 99.8 | 7.3 | 99.9 | 2167 |
| 5.21 - 4.82 | 49893 | 2339 | 21.3 | 44.4 | 99.2 | 6.3 | 99.9 | 2339 |
| 4.82 - 4.51 | 50743 | 2470 | 20.5 | 41.4 | 98.5 | 6.8 | 99.9 | 2470 |
| 4.51 - 4.25 | 51344 | 2590 | 19.8 | 35.6 | 96.9 | 8.1 | 99.9 | 2589 |
| 4.25 - 4.03 | 58307 | 2794 | 20.9 | 29.4 | 99.2 | 10.5 | 99.9 | 2792 |
| 4.03 - 3.84 | 62290 | 2951 | 21.1 | 24.2 | 99.4 | 13.3 | 99.8 | 2950 |
| 3.84 - 3.68 | 65375 | 3077 | 21.2 | 20.1 | 99.6 | 16.8 | 99.7 | 3075 |
| 3.68 - 3.54 | 69088 | 3211 | 21.5 | 14.7 | 99.5 | 23.9 | 99.5 | 3210 |
| 3.54 - 3.41 | 65056 | 3246 | 20 | 10.4 | 97.2 | 33.9 | 98.7 | 3245 |
| 3.41 - 3.29 | 68771 | 3419 | 20.1 | 8.6 | 98.3 | 43.7 | 98.1 | 3410 |
| 3.29 - 3.19 | 74115 | 3545 | 20.9 | 6.7 | 98.5 | 58.4 | 97.1 | 3541 |
| 3.19 - 3.09 | 77528 | 3689 | 21 | 5 | 99 | 86.3 | 95.2 | 3682 |
| 3.09 - 3 | 80755 | 3785 | 21.3 | 3.9 | 99.2 | 98.2 | 92.3 | 3784 |
| 3 - 2.92 | 83501 | 3882 | 21.5 | 3.2 | 99.2 | 119.1 | 90.2 | 3880 |
| 2.92 - 2.85 | 86981 | 4032 | 21.6 | 2.4 | 99.5 | 159.8 | 84.6 | 4032 |
| 2.85 - 2.78 | 79796 | 4035 | 19.8 | 1.7 | 97.6 | 211.8 | 76.3 | 4027 |
| 2.78 - 2.72 | 81918 | 4068 | 20.1 | 1.5 | 98 | 248.9 | 72.4 | 4058 |
| 2.72 - 2.66 | 88905 | 4295 | 20.7 | 1.2 | 99 | 309.1 | 68 | 4292 |
| 2.66 - 2.6 | 92619 | 4377 | 21.2 | 1 | 98.6 | 372.1 | 60.3 | 4375 |
| 2.6 - 2.55 | 94174 | 4438 | 21.2 | 0.8 | 99.1 | 456.9 | 51.1 | 4435 |
| 2.55 - 2.5 | 97212 | 4574 | 21.3 | 0.6 | 99.3 | 628.4 | 38.2 | 4571 |
| 40 - 2.5 | 1659392 | 79820 | 20.8 | 15.6 | 98.7 | 18 | 99.9 | 79755 |

| Type | GS-Hg Bound | | | | | | | |
|---|---|---|---|---|---|---|---|---|
| Resolution Shell (Å) | Total Reflection | Unique Reflection | Multiplicity | Mean (I/sigI) | Completeness (%) | Rmerge (%) | CC1/2 (%) | CC1/2 pairs |
| 40 - 12.75 | 10841 | 641 | 16.9 | 87.1 | 96.7 | 2.9 | 99.9 | 641 |
| 12.75 - 9.02 | 17789 | 1124 | 15.8 | 79.4 | 97.8 | 3 | 100 | 1124 |
| 9.02 - 7.36 | 25433 | 1466 | 17.3 | 58.4 | 99.1 | 4.1 | 100 | 1465 |
| 7.36 - 6.38 | 31591 | 1763 | 17.9 | 37.4 | 99.9 | 6.9 | 99.9 | 1763 |
| 6.38 - 5.7 | 35767 | 1962 | 18.2 | 29.6 | 99.9 | 9.1 | 99.9 | 1962 |
| 5.7 - 5.21 | 33224 | 2095 | 15.9 | 27.4 | 96.5 | 9 | 99.8 | 2092 |
| 5.21 - 4.82 | 40752 | 2331 | 17.5 | 32.6 | 98.8 | 7.9 | 99.9 | 2331 |
| 4.82 - 4.51 | 44714 | 2513 | 17.8 | 31.2 | 99.4 | 8.6 | 99.9 | 2512 |
| 4.51 - 4.25 | 48553 | 2690 | 18 | 27.7 | 99.5 | 10 | 99.8 | 2689 |
| 4.25 - 4.03 | 51938 | 2828 | 18.4 | 22.2 | 99.5 | 13.2 | 99.7 | 2827 |
| 4.03 - 3.84 | 54158 | 2952 | 18.3 | 18.9 | 99.8 | 15.7 | 99.7 | 2952 |
| 3.84 - 3.68 | 48733 | 3009 | 16.2 | 14.7 | 95.9 | 19 | 99.4 | 3004 |
| 3.68 - 3.54 | 55023 | 3204 | 17.2 | 11 | 98.9 | 27.8 | 98.9 | 3201 |
| 3.54 - 3.41 | 59214 | 3360 | 17.6 | 8.3 | 99.3 | 38.8 | 97.8 | 3358 |
| 3.41 - 3.29 | 61809 | 3448 | 17.9 | 6.6 | 99.4 | 50.8 | 96.4 | 3447 |
| 3.29 - 3.19 | 64587 | 3615 | 17.9 | 4.9 | 99.4 | 68 | 94.1 | 3611 |
| 3.19 - 3.09 | 67234 | 3732 | 18 | 3.7 | 99.7 | 94 | 90.2 | 3728 |
| 3.09 - 3 | 68187 | 3793 | 18 | 2.9 | 99.7 | 119.1 | 84.1 | 3792 |
| 3 - 2.92 | 71857 | 3965 | 18.1 | 2.4 | 99.8 | 147.6 | 80.7 | 3964 |
| 2.92 - 2.85 | 63370 | 3900 | 16.2 | 1.7 | 95.7 | 196.6 | 65.6 | 3882 |
| 2.85 - 2.78 | 69640 | 4099 | 17 | 1.4 | 98.3 | 234.6 | 62.2 | 4095 |
| 2.78 - 2.72 | 71722 | 4141 | 17.3 | 1.2 | 99.1 | 285.3 | 52.4 | 4135 |
| 2.72 - 2.66 | 75739 | 4332 | 17.5 | 0.9 | 99.3 | 372.4 | 44.1 | 4326 |
| 2.66 - 2.6 | 78231 | 4414 | 17.7 | 0.7 | 99.5 | 480.4 | 38.2 | 4411 |
| 2.6 - 2.55 | 80339 | 4505 | 17.8 | 0.6 | 99.7 | 566.6 | 26.5 | 4504 |
| 2.55 - 2.5 | 82809 | 4639 | 17.9 | 0.5 | 99.6 | 740.3 | 15.3 | 4636 |
| 40 - 2.5 | 1413254 | 80521 | 17.6 | 12.1 | 99 | 22.7 | 99.9 | 80452 |

| Type | SeMet Bound | | | | | | | |
|---|---|---|---|---|---|---|---|---|
| Resolution Shell (Å) | Total Reflection | Unique Reflection | Multiplicity | Mean (I/sigI) | Completeness (%) | Rmerge (%) | CC1/2 (%) | CC1/2 pairs |
| 40 - 11.91 | 16585 | 806 | 20.6 | 120.6 | 96.4 | 2.3 | 100 | 806 |
| 11.91 - 8.41 | 27689 | 1424 | 19.4 | 98.4 | 96.5 | 2.6 | 100 | 1424 |
| 8.41 - 6.86 | 39683 | 1868 | 21.2 | 62.1 | 99.5 | 4.2 | 100 | 1868 |
| 6.86 - 5.94 | 47387 | 2200 | 21.5 | 37.2 | 99.5 | 7.5 | 99.9 | 2200 |
| 5.94 - 5.31 | 47388 | 2444 | 19.4 | 28.5 | 96.4 | 9.6 | 99.8 | 2442 |
| 5.31 - 4.85 | 57779 | 2743 | 21.1 | 32.6 | 99.4 | 8.7 | 99.9 | 2743 |
| 4.85 - 4.49 | 64051 | 2984 | 21.5 | 29.1 | 99.4 | 10.3 | 99.9 | 2983 |
| 4.49 - 4.2 | 69979 | 3209 | 21.8 | 22.3 | 99.6 | 14.1 | 99.8 | 3209 |
| 4.2 - 3.96 | 71212 | 3393 | 21 | 15.6 | 98.3 | 20.2 | 99.6 | 3389 |
| 3.96 - 3.76 | 68930 | 3519 | 19.6 | 10.3 | 97.7 | 31.7 | 99 | 3514 |
| 3.76 - 3.58 | 78533 | 3750 | 20.9 | 7.1 | 99.1 | 50 | 98.1 | 3750 |
| 3.58 - 3.43 | 83666 | 3953 | 21.2 | 4.2 | 99.4 | 94.9 | 93.7 | 3950 |
| 3.43 - 3.29 | 88052 | 4112 | 21.4 | 2.8 | 99.2 | 140.6 | 88.2 | 4108 |
| 3.29 - 3.18 | 92819 | 4275 | 21.7 | 1.9 | 99.2 | 190.9 | 79.3 | 4272 |
| 3.18 - 3.07 | 95851 | 4404 | 21.8 | 1.2 | 99.1 | 306.7 | 63.9 | 4404 |
| 3.07 - 2.97 | 85448 | 4456 | 19.2 | 0.7 | 96.7 | 515.8 | 43 | 4430 |
| 40 - 2.97 | 1035052 | 49540 | 20.9 | 18.4 | 98.6 | 15.5 | 100 | 49492 |